VASCULAR ENDOTHELIAL CELLS AND PULMONARY EPITHELIAL CELLS: UPTAKE AND RESPONSE TO METAL OXIDE NANOPARTICLES

by

Cassandra Elizabeth Deering Rice

A dissertation submitted to the faculty of
the University of Utah
in partial fulfillment of the requirements for the degree of

Doctor of Philosophy

Department of Pharmacology and Toxicology

The University of Utah

August 2009

THE UNIVERSITY OF UTAH GRADUATE SCHOOL

SUPERVISORY COMMITTEE APPROVAL

of a dissertation submitted by

Cassandra Elizabeth Deering Rice

This dissertation has been read by each member of the following supervisory committee and by majority vote has been found to be satisfactory.

4lpruJkiXWf

N. Shane Cutler

Kent E. Pinkerton

THE UNIVERSITY OF UTAH GRADUATE SCHOOL

FINAL READING APPROVAL

To the Graduate Council of the University of Utah:

I have read the dissertation of Cassandra Elizabeth Rice in its final form and have found that (1) its format, citations, and bibliographic style are consistent and acceptable; (2) its illustrative materials including figures, tables, and charts are in place; and (3) the final manuscript is satisfactory to the supervisory committee and is ready for submission to The Graduate School.

Chair: Supervisory Committee

Approved for the Major Department

William R. Crowley'
Chair/Dean (

Approved for the Graduate Council

Charles A'**Wight**
Dean of The Graduate School

ABSTRACT

Nanomaterials are promoted as a promising technology in highly diverse applications, but concerns about risks of these materials have stimulated extensive research on the adverse effects of manufactured nanoparticles. Our research utilized *ex vivo* tissues to study quantification of unlabeled nanoparticles in biological media and *in vitro* cultures of human cells, treated with suspensions of low-solubility metal oxide materials, to study uptake, cell signaling, and gene regulation. The effects of nanoparticles on the cardiovascular system occur because inhaled nanoparticles may enter systemic circulation, or are directly injected into systemic circulation for medical applications, causing adverse health effects. Silicon dioxide (Si02) particles with sizes between 20-100 nm were used in our studies because they have many commercial and medical applications and can be readily modified with surface functional groups. Our hypothesis is two-fold. First, we hypothesize that tissue uptake and deposition of Si02 nanoparticles can be measured by sedimentation field-flow fractionation (SdFFF) after particle isolation using enzyme digestion. We also hypothesize that the adverse effects associated with nanoparticle exposures are greater in vascular cells than pulmonary and colorectal cell lines, due to the formation of reactive oxygen species, which may stimulate apoptosis. The results presented here demonstrate the cellular uptake of nano and submicron-sized Si02 using the traditional methods of microscopy. Additionally, the method of SdFFF, which is typically used to separate macromolecules, colloids, and

particles, was used in combination with enzyme digestion to provide a novel, useful method to simultaneously measure both the size and concentration of particles in tissues. The toxic effects of metal oxide particle treatment on vascular, pulmonary and colon cells were evaluated. Significant cytotoxicity and inflammation were observed with vascular endothelial cells, but little to no adverse effects were seen in pulmonary and colon cancer epithelial cells at concentrations of 1-316 pg/cm^2. Nano-sized SiO2 caused apoptosis in vascular endothelial cells that was ameliorated by pretreatment with 5 mM of the antioxidant, N-acetyl-L-cysteine. Our results show that exposures of endothelial cells to high concentrations of nano-sized Si02 may have serious adverse cardiovascular consequences. Furthermore, these results provide insights into treatments, such as the use of antioxidants, for persons exposed to significant levels of metal oxide nanoparticles.

This dissertation is dedicated to my family and friends, but most importantly to my mom and dad, and my husband Jonathan

TABLE OF CONTENTS

ABSTRACT....iv

LIST OF TABLES....ix

LIST OF FIGURES....x

LIST OF ABBREVIATIONS....xii

Chapter

1. INTRODUCTION....1

   Definition of a Nanoparticle....1
   Source of Nanoparticle Production....2
   Exposure....7
   Medical and Molecular Consequences of Exposure....17
   Research Objectives....24

2. A NOVEL METHOD TO DETECT UNLABELED INORGANIC NANOPARTICLES AND SUBMICRON PARTICLES IN TISSUE BY SEDIMENTATION FIELD-FLOW FRACTIONATION....26

   Introduction....26
   Methods....27
   Results....32
   Discussion....41
   Acknowledgements....45

3. DIFFERENT VASCULAR AND PULMONARY CELL ADVERSE CYTOKINE RESPONSES TO METAL OXIDE NANOPARTICLES....46

   Introduction....46
   Methods....47
   Results....54
   Discussion....62

4. EVALUATE THE ROLE OF APOPTOSIS AND REACTIVE OXYGEN SPECIES IN ENHANCED SUSCEPTIBILITY OF VASCULAR CELLS....70

Introduction....70
Methods....71
Results....73
Discussion....79

5. CONCLUSIONS....84

Overview....84
Chapter 2....85
Chapter 3....87
Chapter 4....88
Future Directions....89
Final Statement....90

REFERENCES....92

LIST OF TABLES

Table		Page
1.1	Uses for nanoparticles	4
3.1	Cell types used in this study	48
3.2	Metal oxide particles used in this study	50
3.3	LD_5O (|ig/cm^2) of metal oxide nanoparticles treated cells	57
3.4	Concentration resulting in statistically significant IL-6 production (ng/cm)	61

LIST OF FIGURES

Figure		Page
1.1	Deposition of particles in the lung	9
1.2	Separation of particles by FFF	12
1.3	Sedimentation FFF (SdFFF) instrumentation	13
1.4	Plausible particle exposure concentrations	16
1.5	Proposed pathway of cardiovascular toxicity of MPs	20
2.1	Schematic of the tissue sample preparation protocol	28
2.2	Uptake of 100-nm $Si0_2$ into HAECs	33
2.3	Fractograms of 70-nm $Si0_2$ particles injected at different concentrations	35
2.4	Tracking the particles through the isolation procedure	36
2.5	SdFFF fractogram of 70-nm Si02 nanoparticles extracted from lung cells	38
2.6	Bimodal distribution of 70 and 250-nm particles	39
3.1	Schematic diagram of real-time PCR process	52
3.2	Cytotoxicity of metal oxide nanoparticles in HAECs	55
3.3	Cytotoxicity of metal oxide nanoparticles in BEAS-2B cells	56
3.4	IL-6 protein release from HAECs	59
3.5	IL-6 protein release from NHBEs	60
3.6	Cytokine gene induction in vascular cells	63
3.7	The cytokines IL-6 and IL-8 gene induction in NHBEs	64

4.1 Apoptosis - Annexin V-FITC diagram....72

4.2 Representative cell gating by flow cytometry for the untreated control....74

4.3 Percent HAECs in each quadrant after treatment with 10 nm SiC>2....76

4.4 Apoptosis in vascular cells treated with Si02....77

4.5 Apoptosis in BEAS-2B cells....78

4.6 Evaluating the role of ROS in HAEC apoptosis....80

LIST OF ABBREVIATIONS

Al_2O_3	aluminum oxide
Apaf-1	apoptotic protease activating factor-1
ANS	autonomic nervous system
ASTM	American Society for Testing and Materials
ANS	autonomic nervous system
ATCC	American Type Culture Collection
AV	annexin V
BEAS-2B	Human Bronchial Epithelial Cell Line
BEGM	bronchial epithelial growth media
°C	degrees Celsius
CaO	calcium oxide
CB	carbon black
CCK-8	Cell Counting Kit-8
cDNA	complementary deoxyribonucleic acid
CeO_2	Cerium IV Oxide
CO_2	carbon dioxide
Cr_2O_3	chromium oxide
CRP	C-reactive protein
DAPI	4',6-diamidino-2-phenylindole

DMEM ..... Dulbecco's Modified Eagle Medium

DMTU 1,3-dimethyl-2-thiourea

DNA ..... deoxyribonucleic acid

EGM-2 ..... endothelial growth medium-2

ELISA ..... Enzyme-Linked Immunosorbent Assay

EPA ..... Environmental Protection Agency

Fe_2O_3 ..... iron (III) oxide

FFF ..... field-flow fractionation

GI ..... gastrointestinal

GM-CSF ..... granulocyte macrophage colony-stimulating factor

GST ..... glutathione S-transferase

HAEC ..... Human Aortic Endothelial Cells

H_2O ..... water

H_2O_2 ..... hydrogen peroxide

HOCl ..... hypochlorous acid

HUVEC ..... Human Umbilical Vein Endothelial Cells

IACUC ..... Institutional Animal Care and Use Committee

ICP-MS ..... inductively coupled plasma mass spectroscopy

IL-ip ..... interleukin-ip

IL-6 ..... interleukin-6

IL-8 ..... interleukin-8

LD_{50} ..... half maximal lethal dose

LHC-9 ..... Lechner and LaVeck media

LIF ..... leukemia inhibitory factor

i.v. ..... intravenous

μg ..... micro-gram

MgO ..... magnesium oxide

μl ..... micro-liter

μM ..... micro-molar

min ..... minute

ml ..... milli-liters

mM ..... milli-molar

mRNA ..... messenger ribonucleic acid

NAC ..... N-Acetyl-L-cysteine

NF-κB ..... nuclear factor-κB

NiO ..... nickel oxide

NMMAPS ..... National Mortality and Morbidity Air Pollution Study

NHBE ..... normal human bronchial epithelial cell line

NO· ..... nitroxyl radical

NP ..... nanoparticle

NQO1 ..... NAD(P)H dehydrogenase, quinone 1

O_2^- ..... superoxide radical

·OH ..... hydroxyl radical

PBS ..... phosphate buffered saline

PCR ..... polymerase chain reaction

PI ..... Propidium Iodide

	particulate matter
PM	coarse particulate matter
PM2.5	fine particulate matter
PMo,	ultrafine particulate matter
PS	phosphatidyleserine
RNA	ribonucleic acid
RO'	alkoxyl radical
ROO-	peroxyl radical
ROOH	hydroperoxide
ROS	reactive oxygen species
RT-PCR	reverse transcription-polymerase chain reaction
SdFFF	sedimentation field-flow fractionation
sec	seconds
SI	international system of units
SOD	superoxide dismutase
$Si0_2$	silicon dioxide
SE	standard error
TEM	transmission electron microscopy
Ti02	titanium dioxide
TNF-a	tumor necrosis factor-a
UFP	ultrafine particles
WGA	wheat-germ agglutinin
ZnO	zinc oxide

CHAPTER 1

INTRODUCTION

Definition of a Nanoparticle

The SI (international system of units) definition of nano is a prefix used to form decimal submultiples of the SI unit "meter", designating a factor of 10^{-9} denoted by the symbol "n". The word particle is defined as a small object that behaves as a whole unit in terms of its transport and properties. However simply combining these two terms together does not truly define a nanoparticle. According to the American Society for Testing and Materials (ASTM), an international standards organization, a nanoparticle is a sub-classification of ultrafine particle with lengths in two or three dimensions greater than 1 nm and smaller than 100 nm, which may or may not exhibit size-related properties [1]. This definition is based on the field of nanotechnology. However, since the study of nanoparticles is interdisciplinary, the term nanoparticle is often confused with other terminology such as ultrafine particles (UFP) and nucleation mode particles [2]. Oberdorster *et al.* reviews the classification of nanoparticles based on size and origin as viewed by a toxicologist, an atmospheric scientist and a material scientist [3]. Since the term nanoparticle is so complex, the definition of a nanoparticle used henceforth will be based on size as defined by the ASTM where particles smaller than 100 nm are called nanoparticles (NPs).

Source of Nanoparticle Production

Incidental and Environmental

The source of nanoparticle production can be classified as either incidental/environmental or anthropogenic/manufactured. Incidental and environmental particles are the principle components of air pollution. Studying the effects of air pollutants is a major focus of the Environmental Protection Agency (EPA) because of a growing link between air pollution and morbidity and mortality. The first piece of evidence linking air pollution and mortality was in the Meuse Valley in 1930, where during a pollution episode, 60 people died within 3 days [4], The "London Fog" of 1952 provided additional epidemiological data correlating mortality and air pollution [5]. More recently, the National Mortality and Morbidity Air Pollution Study (NMMAPS) of the 90 largest U.S. cities, estimated that the daily total and cardiopulmonary mortality increased in the short term by 0.21% (±0.06 standard error (SE)) and 0.31% (±0.09 SE), respectively, for each 10 pg/m^3 increase in coarse particulate matter (PMio) measured over a 24-hour period [6]. Because 24-hour PMio concentrations within the U.S. range from a low of 24 to a high of 719 pg/m^3 [7], cumulative risk from particulates can be substantial in some regions of the country.

Air pollution consists of a heterogeneous mixture of gases, (NO2, CO, SO2 and ozone) and particulate matter (PM). Suspended particles are generally separated into coarse (PM10-2.5), fine (PM2.5) and ultrafine ($PM_{0}.i$) fractions [8]. Primary particles in air pollution are emitted directly into the environment, but secondary particles, such as nitrates and sulfates, are formed from gaseous nitric acid and sulfur dioxide. PM10-2.5 arise almost exclusively from natural sources, like windblown soil, and from other sources like tire fragmentation, resuspension of road dust, smelting, processing, agriculture, construction and

demolition activities, pollens, molds and volcanic emissions. PM2.5 and PM_{0}.i particles arise almost exclusively from combustion, and are comprised of motor vehicle emissions, power generation and other industrial combustion products (including smelter emissions), and residential wood burning and forest fires. A study of the air in Houston was performed to determine exposures of the population on a daily basis [9]. The results show particulates such as carbon black (CB), which is often used as a surrogate for combustion soot, and many other particulates were present in the air. Interestingly, they found that nano-sized silica, not typically found in the air, was also present. The source of nanosilica in the air is most likely from an incineration process or perhaps through thermal decomposition of silane [10],

Anthropogenic and Manufactured

With the advances in technology and the attractiveness of nanoparticle chemistry, scientists have begun to introduce nanoparticles into various scientific fields. Already there are over 600 manufacturer-identified consumer products incorporating nanotechnology [11]. A few of the current and future uses for nanoparticles are summarized in Table 1.1. The National Nanotechnology Initiative (NNI) was developed by the National Science and Technology Council (NSTC) to coordinate science and technology policy at the level of the Federal Government. The NNI has identified and outlined the needs for research related to environmental health and safety of nanomaterials. Their strategy for nanotechnology research is outlined in a report by the NSTC [12]. In general the federal government has realized the growing use of nanomaterials and has developed an agency to oversee and regulate funding for the advancement of the environmental health and safety of nanoparticles.

Table 1.1 Uses for nanoparticles

Biomedical, pharmaceutical cosmetic applications	Energy, catalytic structural applications
• Antimicrobials • Bio-detection and labeling • Bio-magnetic separations • Drug delivery • MRI contrast agents • Orthopedics and implants • Sunscreens • Thermal spray coatings	• Automotive catalyst • Ceramic membranes • Fuel cells • Photo-catalysts • Propellants • Scratch-resistant coatings • Structural ceramics • Solar cells

Metal Oxide Nanoparticles

Metal oxides comprise a very important category of nanoparticles which can impact human health through environmental and manufactured processes [13]. Metal oxide nanoparticles can be prepared with extremely high surface areas and can form unusual crystal structures that have multiple reactive surface features, including edges and corners [14]. These reactive surfaces can facilitate interesting reactions, e.g., methane activation, **D2**-CH exchange, CO oligomerization, oxygen exchange in CO2 and H2O [15]. The nanostructures of metal oxides can exhibit an electronic arrangement that can display metallic, semiconductor, or insulator characteristics. Insulating oxides contain metals from Groups I, II and XIII-XVII of the periodic table (MgO, CaO, $A1_20_3$, and Si02), while semiconducting or metallic oxides contain metals from groups III-XII of the periodic table (ZnO, Ti02, NiO Fe203 and C^Oa). Transitional metal oxides (Ru, Mo, W, Pt, V) are used as catalysts and sensor materials [15]. Applications for metal oxides include fabrication of microelectronic circuits, sensors, piezoelectric devices, fuel cells, coatings for the passivation of surfaces against corrosion, and catalysts [13].

Drug Delivery

In addition to their use as components of electronics, metal oxides are useful in the biomedical field as vehicles for drug [16-18] and gene [19, 20] delivery, as well as imaging probes [21] and as disease diagnostic tools. Use of these and other particulates in the biomedical field has spawned a new term, nanomedicine. Nanoparticles were chosen for use in the medical field because of their unique properties, which make them different from the corresponding bulk materials of the same chemical composition. A notable difference between micron and nano-sized particles is their surface area per mass. Klabunde *et al.*

compare surface atoms and bulk atom ratios that are based on particle size, to show that spherical nanoparticles (less than 3 nra) have more of the atoms or ions on their surfaces [14]. Due in part to the large and reactive surface areas of nanoparticles, drugs can be conjugated to their surface to achieve high concentrations and site-specific dosing [3]. Being able to conjugate drugs to the particle surface permits for high concentrations of drug to be delivered to a specific site. However, an additional benefit of nanoparticles is that their increased surface reactivity can lead to increased uptake and interactions with biological tissues [22], This method of drug delivery would be less interesting if the particle-drug conjugates were not able to enter the tissue of interest.

The properties that make nanoparticles attractive carriers also increase their toxicities. The increased surface area and reactivity means the particles can adsorb other particles, proteins or chemicals on their surface, which changes their interactions with cells. Increased uptake may be desirable if the particle reaches the right location for drug delivery. However, the particle may enter other tissues and cause toxicity. Only a limited number of studies have investigated the interactions of nanoparticles, used in the medical field, with human-derived cells, so the potential for toxicity is not well understood. Evidence from air pollution-focused studies show that insoluble nano-sized particles can translocate from the lung to the blood stream [20, 23, 24] and can causes adverse cardiovascular effects resulting in morbidity and mortality in susceptible populations [6, 25].

Doses of injected particles in the vasculature for biomedical purposes will be much higher than air pollution exposures. The interaction between Si02 and the heart and blood vessels may compromise this organ system. Previous studies by Martin *et al.* [26] showed acute toxicities in mice after an injection of micron sized Si02 particles used in drug delivery.

Showing minor toxicities in healthy mice is the first step for assessing particle safety, however persons receiving these drug treatments are most likely not healthy. The effects of these drug conjugates in a compromised animal model would simulate the responses of individuals in different diseases states. Scientists who study drug delivery with conjugated nanoparticles recognize the potential for adverse events and are slowly working to ensure toxicities are identified before the therapy is introduced to patients [27]. In fact, Kim *et al.* examined the toxicity and tissue distribution of silica-overcoated magnetic nanoparticles injected into mice. Particles were found in most organs of the mouse but no significant toxicities were identified by analyzing markers in the serum [28]. In contrast to product-specific safety testing, such as needed to plan clinical trials, research focusing on the fundamental molecular mechanisms of particle interactions with cells is needed. In more mechanistic studies, Chen *et al.* reported human epithelial cell uptake and translocation of nano-sized silica particles to the nucleus where the particles induced formation of aberrant clusters containing proteins that are important in gene regulation [29]. Furthermore, silica-nuclear protein clusters were shown to inhibit replication, transcription, and cell proliferation [29]. Mechanistic understanding of particle-vascular cell interactions can help predict adverse events that may occur and can guide development of biocompatible formulations.

Exposure

Exposure to nanoparticles can vary depending upon the particulate source. Dermal exposures are often intentional through the application of sun screen, which contains zinc oxide (ZnO) and/or titanium dioxide (TiC^), and topical cosmetics. However, dermal absorption of these particles has yet to be established since the skin provides a thick protective barrier [30]. Ingestion, exposing the gastrointestinal tract (GI), is another common

route of exposure. Ingestion can be accidental due to ingestion of topically applied nanoparticles, foods that use nanoparticles such as Ti02 as food additives [31] to improve food flavor, color, or texture or by clearing inhaled particles from the lung by coughing followed by ingestion. Injection of particles into the systemic circulation is most often related to the use of nanoparticles for biomedical purposes. However, translocation of particles into systemic circulation leads to vascular exposure. The most common route of exposure is by inhalation (respiratory tract). A source of inhaled nanoparticles is from air pollution but can also be from inhaled drugs using nanoparticles as drug carriers.

Uptake and Translocation

All fractions of inhaled particulates are capable of reaching the respiratory tract. Figure 1.1 graphically represents the alveolar space in the lung drawn to scale. Particles are drawn in the alveolar air space at sizes from 10 nm to 5 pm. It becomes clear that larger particles would tend to deposit in the upper respiratory tract and tracheobronchial regions, and small particles (PM2.5) would show greater deposition in lower airways. Ultrafine or nano-sized particles (PM0.1) are short-lived because of a tendency to coalesce, but deposit in the tracheobronchial and alveolar regions and are, therefore, potentially the most toxic. The graph in the bottom corner of Figure 1.1 depicts the deposition of particles based on size in the alveolus; the smaller the particles, the higher the deposition.

As shown in Figure 1.1, nanoparticles are very small relative to the alveolar epithelial cells, and are believed to enter the systemic circulation from the lung [22, 24, 32-35]. Current hypotheses for the method of translocation are as follows: 1) cell mediated active transport via phagocytosis (macrophages) and/or endocytosis (alveolar epithelial or endothelial cells), 2) passive transportation/diffusion, or 3) by active or passive transport

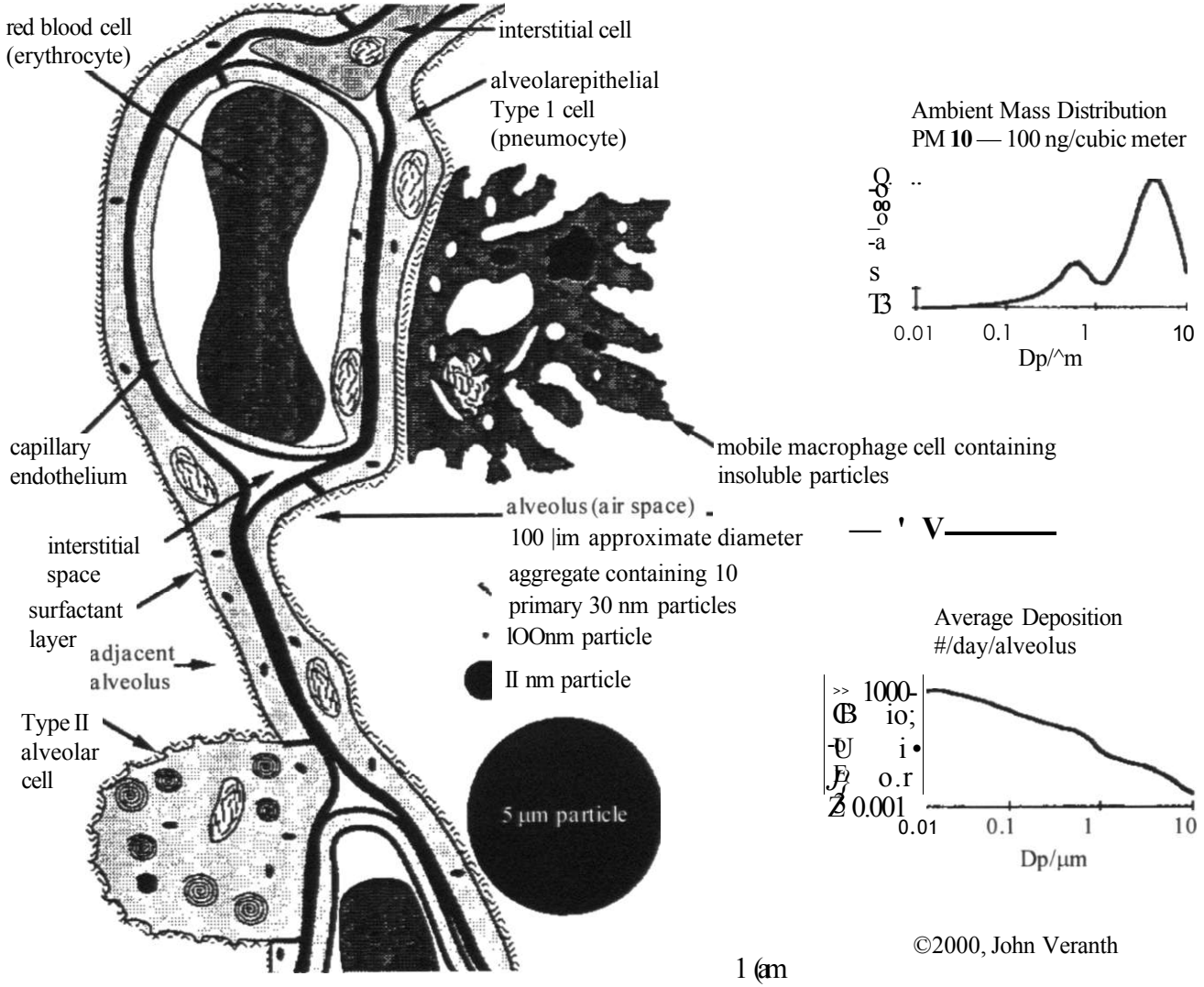

Figure 1.1 Deposition of particles in the lung. Reproduced with permission from John Veranth (Copyright 2000).

through pores (caveolae) in the cytoplasm of endothelial cells or between epithelial cells (gap junctions) [36].

Monitoring human exposure to engineered nanoparticles (from air, water, food, consumer products, and soil), determining the rate of particle uptake by humans and food chain organisms, and measuring the resulting nanoparticle concentrations in target organs are major challenges for nanoparticle toxicology studies [37], Most nanoparticle uptake and translocation research has quantified nanoparticles *in vivo* using some type of unique particle label. Kreyling *et al.* showed translocation of 15- and 80-nm radio-labeled iridium particles in rats with deposition outside of the lung being less than 1% [24]. Sadauskas *et al.* used trace metals such as gold and iridium [38], and Ryman-Rasmussen *et al.* used fluorescent particles [39] to determine particle translocation. However, the population exposures most relevant to health of the general population involve the emissions or deliberate release of high-production-volume manufactured nanomaterials and exposures to incidental nanoparticles, such as soot. Combustion emissions and manufactured powders such as fumed silica, ultrafine TiC>2, and similar industrial materials rarely have a unique and easily detected label.

Without using a unique label, Geiser *et al.* showed that 22 nm Ti02, instilled into rats, was found on the luminal side of airways and alveoli, in all major lung tissue compartments and cells, and within capillaries, using energy filtering transmission electron microscopy (TEM), [22]. Furthermore, Elder *et al.* used elemental analysis to show the presence of inhaled 30 nm manganese particles in neural tissue [40]. Measuring changes in the concentration of unlabeled particles in tissue with these techniques is difficult. Extracting quantative information from TEM images is inexact and elemental analysis does not

distinguish particles from soluble forms and provides no information on particle size. A more quantitative and qualitative method is needed to determine particle deposition.

A promising method to measure size and concentration of unlabeled nanoparticles is through separation by field-flow fractionation (FFF), which was first developed in the 1960s for separating macromolecules, colloids, and particles [41, 42], FFF has been used for the measurement of numerous properties of macromolecules and colloidal particles, including particle mass, size, and density. Caldwell *et al.* reported seminal work applying FFF to detect protein-based particles in eye lens cataracts [43]. FFF has been used to characterize natural aquatic colloids [44-46], and perform size separation of single-walled carbon nanotubes [47].

FFF is similar to chromatography methods in that materials are separated by transport velocity, but in place of a retention media the separation is carried out in a thin, open channel with bulk flow in the longitudinal direction and a separation field (centrifugal force, electric field, thermal gradients, or cross-flow) in the perpendicular direction. Particles are driven to the wall by the separation field and average particle distance from the wall is determined by the competition between the separation field and the size-dependent diffusion of particles against the concentration gradient. Since the narrow channel has a parabolic flow profile (laminar flow), the particles farthest from the wall are in the highest velocity streamlines and therefore travel the fastest. Figure 1.2 demonstrates separation of particles using FFF. With normal FFF as shown in figure 1.2, smaller particles elute first because they are furthest from the collection wall and in the fastest field of the carrier fluid flow velocity. Sedimentation FFF (SdFFF) uses centrifugal force to generate the separation field. Figure 1.3 depicts an

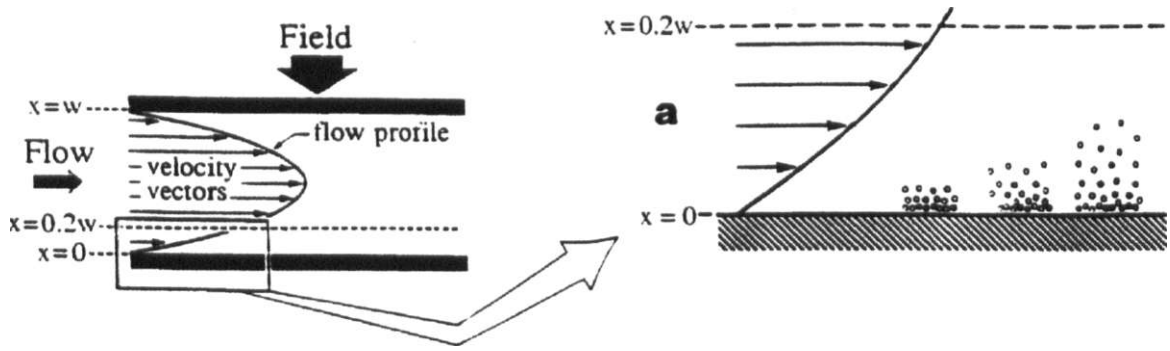

Figure 1.2 Separation of particles by FFF. Normal FFF, used to describe the separation of particles with a diameter of less than 1 pm. Smaller particles elute first. Reprinted with permission of Wiley-Liss, Inc. a subsidiary of John Wiley & Sons, Inc. [42]

Figure 1.3 Sedimentation FFF (SdFFF) instrumentation. Reprinted with permission of Wiley-Liss, Inc. a subsidiary of John Wiley & Sons, Inc. [42]

SdFFF instrument. The minimum detectable particle size depends on the particle density and the maximum centrifugal force of the SdFFF instrument [48, 49]. Giddings provides a full derivation of the governing equation and a graph of minimum resolvable diameter versus GAp for a typical instrument channel geometry [50]. For example, silica particles with a density of 2.0-2.65 g/ml, particles as small as -22 nm can be separated using a SdFFF instrument's maximum centrifugal force. For denser particles such as gold, applying the same field can separate particles as small as 10 nm. Multiple detection techniques can be used simultaneously with FFF, including fluorescence, ultra-violet absorption, light scattering, and inductively coupled plasma mass spectroscopy (ICP-MS). The advantage of coupling the FFF instrument to ICP-MS is the enhanced sensitivity of the detector as well as its capability to determine the composition of the particles collected.

Dosimetry

Calculating the theoretical concentration of particle exposure *in vivo* and extrapolating this to an *in vitro* dose is very complicated. Methods for *in vivo* dose calculation can be found in Veranth *et al.* [51]. Veranth *et al.* estimated the inhaled volume of particulates to be 10 m^3/day for high environmental exposures and a reasonable concentration for occupational exposure [51]. The deposition of nanoparticles in the lung is estimated at about 60% based on ICRP estimates [52]. The calculated dose based on the area of the lung (70 m [53]) is 0.08 ng/cm . As stated earlier, particles of different sizes deposit in different areas of the lung leading to the accumulation of particles at high concentrations in certain areas of the lung [54], Figure 1.4A shows the estimated particle dose based on the known average volume of the lung and the assumption based on exposure. The range is from 0.08 ng/cm^2 (based the calculated inhaled exposure) to 80 ng/cm^2 which takes into account

uncertainties of deposition, and airflow, with high concentrations of particles depositing in certain sites of the lung. Figure 1,4B depicts the same data plotted based on the average volume of lung surfactant.

The same analysis was performed based on the dose of particles in the blood, either from translocation from the lung (estimated at less than 1% [24]) or from injection as drug carriers or imaging agents. Doses based on translocation are relatively small, however doses used for MRI contrast agents and chemotherapy drugs would be much higher. Ingestion and dermal exposures are also shown. Figure 1.4 shows these estimated values.

Dosimetry as discussed so far has focused on *in vivo* exposures. The extrapolation of these doses to a survey of previous *in vitro* study doses is represented as the gray bars in Figure 1.4. The doses of particles used for *in vitro* studies are often higher than the plausible dose in regards to area dose and more reasonable for a per volume dose. Many assumptions are made to simplify the calculations of both exposures. For *in vitro* studies using cell culture models, one of the main artifacts that differ from *in vivo* studies is settling velocity which may alter the actual dose that the cell encounters. For *in vivo* studies, particle deposition may occur in the lung, however for other tissues, particles are being carried by the blood, over the endothelial cells and may further deposit in multiple target (vascularized) tissues. In cell culture, particles are suspended in culture medium and allowed to settle, diffuse, agglomerate onto the cells. For this reason, Teeguarden *et al.* introduced the term particokinetics [55]. The properties that determine the particokinetics of a particle in culture medium are as follows: media density and viscosity as well as particle size, shape, charge and density. The dose of the particle that interacts with the cells is likely determined by these physical properties. Teeguarden *et al.* calculated the theoretical time needed for various

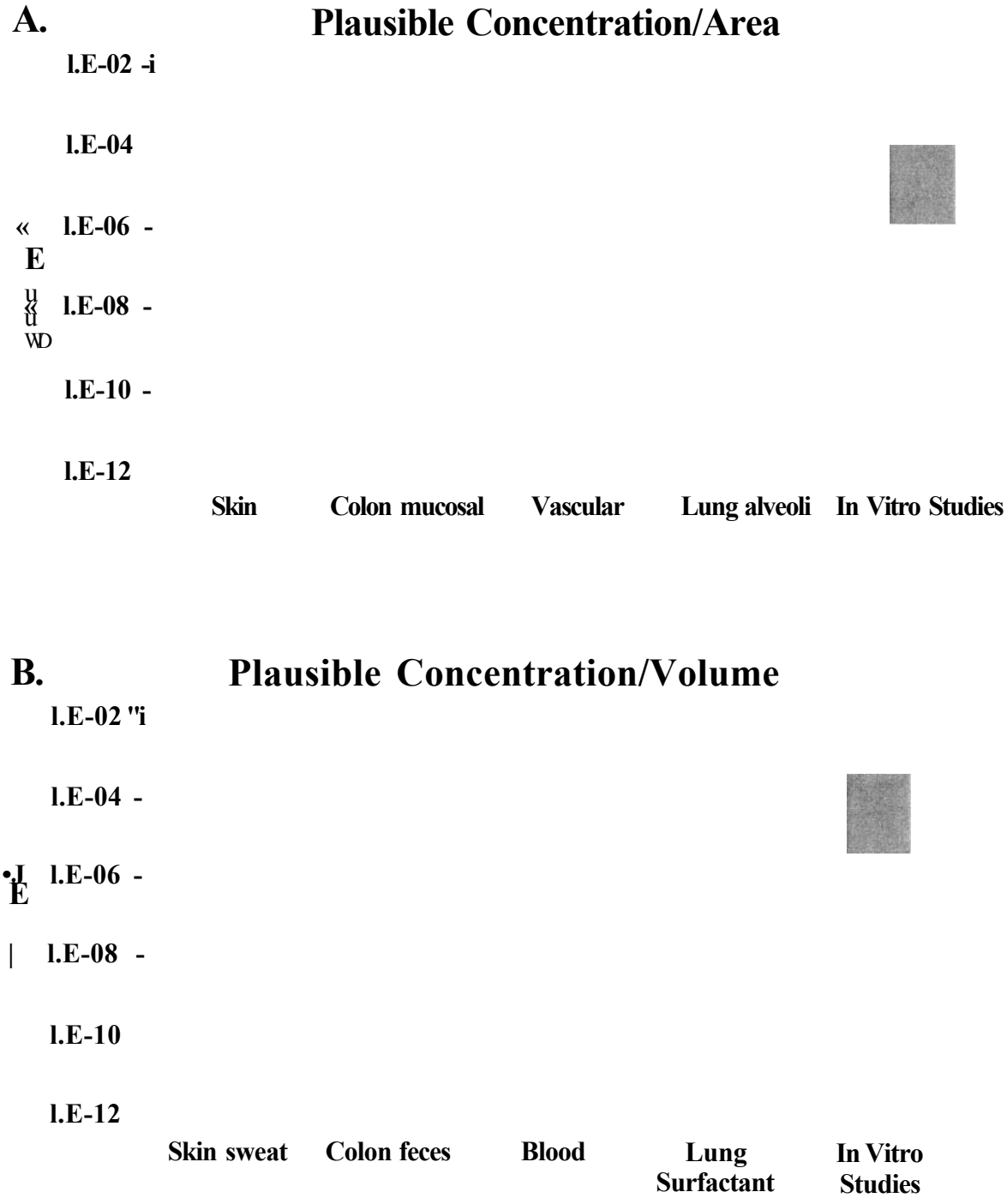

Figure 1.4 Plausible particle exposure concentrations. *In vitro* concentrations are represented as a gray bar. Redrawn from data in Veranth *et al. [51].*

particles to travel 1 mm by settling and diffusion [55]. It is estimated that 50-nm silica nanoparticles would take 17 days to settle to the bottom of a culture dish interacting with cells, however cytotoxicity has been shown at 24 hours. The toxicity of particles often assumes direct contact of the particles with the cells, however toxicity may be due to interactions with dissolved molecules from the surface of the particle. Over time, depending on the rate of settling and diffusion, the interaction of particles with cells will increase leading to enhanced particle effects. Lison *et al.* tested the particokinetics theory using Stober nanoparticles, which are soluble and do not settle according to the diffusion/gravitational settling model of Teeguarden *et al.* [55] and still showed significant cytotoxicity at 24 hours [56]. Therefore, they believe that the nominal dose and particle concentrations are the most important determinants of cellular effects, not the effects of settling [56].

The theory of particokinetics is relatively new. However it may explain the differences between *in vitro* particle research between laboratories that utilize slightly different methodologies. Standardization in the field of particle toxicology is therefore needed. Further understanding of particokinetics can aid in the comparison of existing toxicology studies.

Medical and Molecular Consequences of Exposure

Toxicity and Inflammation

Cytokines are soluble peptides that regulate many signal transduction pathways, cell growth, differentiation, and apoptosis, as well as recruitment signals for neutrophils, macrophages, and other mobile cells to specific sites [57]. Cytokines exert their regulatory effects by binding to specific receptors belonging to the cytokine superfamily [57]. The

function of each cytokine varies but they all play an integral role in the coordination and persistence of inflammatory processes. The majority of toxicology studies are based on air pollution exposures. Particulates found in ambient air pollution have been shown to induce a lung inflammatory response in humans [58, 59] characterized by direct activation of nuclear factor-KB (NF-KB) in the airway epithelium [60, 61], with increased expression of intracellular adhesion molecule-1 [61] and enhanced production of interleukin-ip (IL-1|3) [62], interleukin-6 (IL-6) [60-62], interleukin-8 (IL-8) [58, 61, 62], leukemia inhibitory factor (LIF) [62] and granulocyte macrophage colony-stimulating factor (GM-CSF) [62], Particulates also secondarily prime a pro-inflammatory response in lung epithelium by inducing secretion of tumor necrosis factor-a (TNF-a) by alveolar macrophages [63]. Pulmonary deposition of particulates stimulates bone marrow monocyte release [64] and facilitates experimental thrombosis [65] in animals. In healthy humans, particulate exposure increases blood fibrinogen levels [58] and C-reactive protein (CRP) [66] and causes acute arterial vasoconstriction [67]. Thus, inflammatory mediators produced locally in the lung by inhalation of particulates readily spill over into the systemic circulation from the pulmonary circulation. Considering the important role inflammation plays in the pathogenesis of atherosclerosis [68] and acute plaque rupture, leading to coronary thrombosis [69], it is not surprising that one of the major consequences of particulate air pollution exposure is an increase in both short- and long-term cardiovascular events and mortality [25]. Figure 1.5 shows the proposed mechanisms by which NPs may lead to cardiovascular dysfunction. Pulmonary inflammation, which has already been described, can cause systemic inflammation leading to the activation of platelets and leukocytes as well as activation of an acute phase response. Particles may also translocate and directly interact with the

vasculature leading to local inflammation. Furthermore, inhaled particles may alter the autonomic nervous system. Particulate exposure has been shown to increases the risk of ST-segment depression, a measurement of the repolarization of the ventricles of the heart, during submaximal exercise testing; suggesting that exposure to air pollution particles contributes to myocardial ischemia in subjects with coronary disease [70]. Particulate exposure by inhalation also appears to trigger myocardial infarction in susceptible individuals [71], consistent with the development of a pro-inflammatory, pro-coagulant systemic state. In addition, disturbances of cardiac rhythm are precipitated by particulates, placing subjects with cardiac arrhythmias at risk. Clearly, particulate air pollution represents an important challenge to those concerned with protecting public health.

Apoptosis and ROS

To understand the mechanism by which particles alter cellular functions, the endpoints of apoptosis and its relationship to reactive oxygen species (ROS) will be examined. Apoptosis is classically defined as programmed or "planned" cell death that is part of normal homeostasis. This mode of cell death occurs in an organized manner, resulting in adjacent cells engulfing and degrading packaged contents of the dying cell. Inflammation is not caused by apoptosis as it is for methods of cell death leading to necrosis, which is "unplanned" and "unorganized" resulting in the uncontrolled release of cellular contents. The activation of apoptosis can occur through external or internal pathways. Extracellular signals can include: hormones, growth factors, nitric oxide, and cytokines, and therefore must either cross the plasma membrane or activate cell membrane signal transduction cascades to elicit a response [72]. Intracellular apoptotic signaling is initiated by a cell in response to stress, such as DNA damage, hypoxia, viral infection, or heat [72].

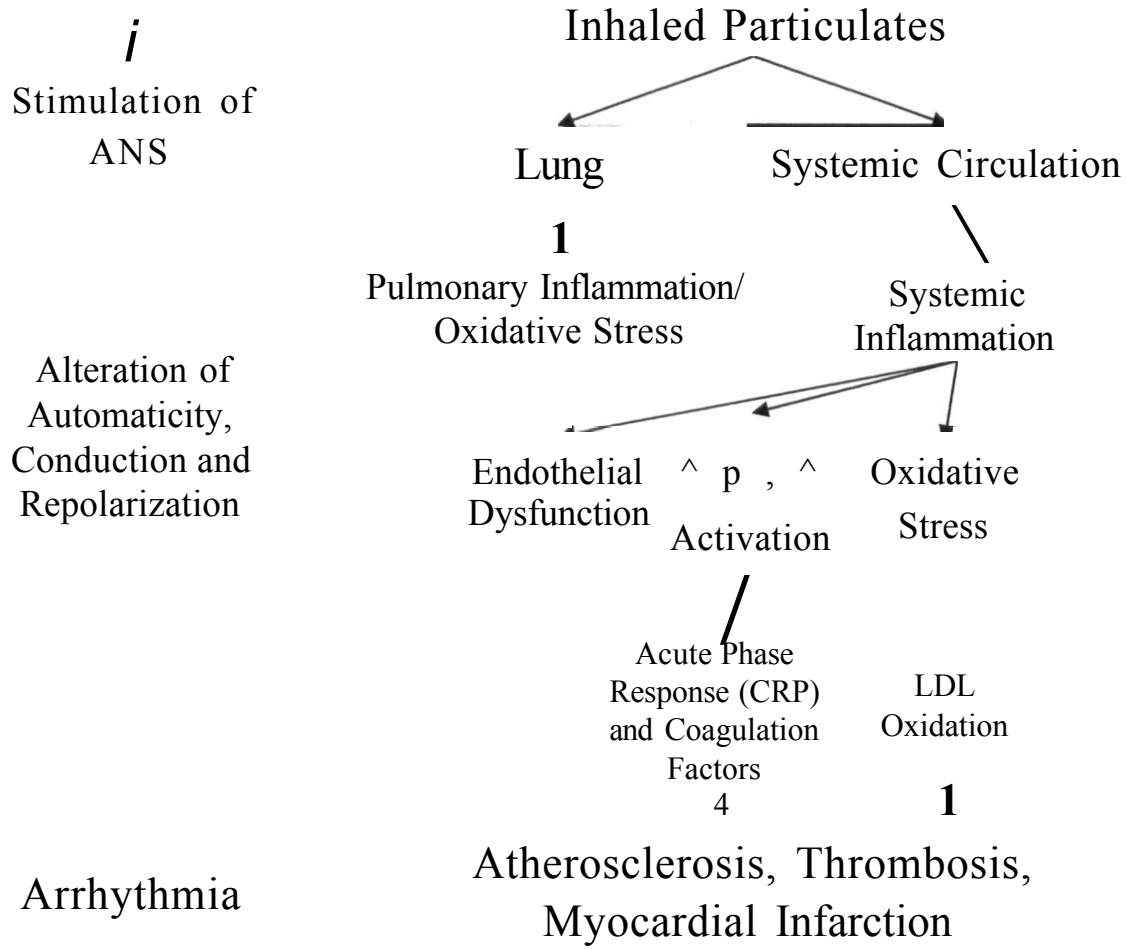

Figure 1.5 Proposed pathway of cardiovascular toxicity of NPs.

Determining the cause of apoptosis, be it activation of the internal or external pathway, may give insight into the mechanism by which particles cause cell death. Many pro-death stimuli are closely associated with mitochondrial function. Bcl-2 proteins on the surface of the mitochondria detect damage, and activate Bax proteins, which destabilize the mitochondrial membrane, causing cytochrome c to be released. Cytochrome c binds to apoptotic protease activating factor-1 (Apaf-1) forming an apoptosome [73]. The apoptosome binds to and activates caspase-9 and the caspase cascade, which cleaves the proteins of the mitochondrial membrane, causing it to break down and start a chain reaction of protein denaturation and eventually phagocytosis of the cell [73], Activation of the various caspases is not solely through mitochondrial release of cytochrome c. Activation of cellular receptors, such as the TNF-a receptor, activates caspase-8 [72], The complete signaling pathway for apoptosis is too complicated to be reproduced here, but has been reviewed by Kumar [74].

The methods for detecting apoptosis focus on the cellular alterations being induced. These techniques include measuring mitochondrial versus nuclear DNA degradation, detecting morphological changes via microscopy, determining DNA damage, assessing alterations in nuclear chromatin, analyzing changes in mitochondrial transmembrane potential, measuring the externalization of phosphatidylserine (PS), measuring DNA strand breaks, analyzing sphingolipids, and measuring caspase activation [72]. The best technique to use is debatable and the majority of the time these techniques are used in combination. The technique that will be used in this dissertation is the measurement of PS externalization, one of the early changes that occur during apoptosis. Externalization of PS has not been linked directly to the activation of the internal or external pathways. What is known is that

externalization is regulated by calcium-dependent phospholipid scramblase activity and inactivation of aminophospholipid translocase [75]. The externalization of PS is responsible for the recruitment signal for phagocyte docking and subsequent engulfment and degradation of apoptotic cells. Assaying apoptosis with this technique is therefore useful for determining if cells are undergoing apoptosis. Assays focusing on more mechanistic aspects of apoptosis such as external versus internal pathway activation will determine the cause of apoptosis.

Reactive oxygen species are ions or small molecules that include hydroxyl (OH), alkoxyl (RO), peroxyl (ROO), superoxide (0_2) and nitroxyl radicals (NO). Non-radical ROS include hydrogen peroxide (H2O2), organic hydroperoxides (ROOH) and hypochlorous acid (HOC1). Oxygen-derived free radicals are generated during many naturally occurring cellular processes such as oxidative metabolism and energy production [76]. Reactive oxygen species are also produced in response to cytokines or growth factors and are involved in regulation of signal transduction, gene expression, activation of receptors and nuclear transcription factors, and oxidative damage to cell components [76]. ROS are implicated in many disease processes such as cancer, aging and age related degenerative diseases such as Alzheimer's disease [77-79] and cardiovascular diseases such as atherosclerosis [80],

Antioxidants are often treatments for diseases where ROS are involved. Common antioxidants include Vitamin C, Vitamin E, glutathione, and melatonin. Other mechanisms for detoxifying ROS are cellular enzymes. These proteins include superoxide dismutase (SOD), NAD(P)H:quinone oxidoreductase (NQOl), catalase and peroxiredoxins. Antioxidants detoxify reactive oxygen species by removing free radical intermediates, and inhibit further oxidation reactions by being oxidized themselves. Garewal provides a review of antioxidants used in disease prevention [81].

Other causes of ROS production is exposure to particulate matter. The surface of particles themselves can be reactive producing ROS either intracellularly or extracellulary [82-85]. In addition to the capacity of particles to produce ROS directly, cellular systems produce ROS in the presence of particles. When particles are inhaled, immune cells are activated, responding to particles as foreign bodies leading to the production of inflammatory mediators as well as ROS [86]. Furthermore, particles are known to adsorb proteins and other chemicals which may enhance their uptake or contact with cell [86]. Other mechanisms of particle-induced ROS formation are currently under investigation.

Oxidative stress is often viewed as a component in the inflammatory response signaling cascade and the stimulation of adhesion molecules and chemoattractant production [76]. Furthermore, ROS has been linked to apoptosis. An early study by Pierch *et al.* showed that treatment of cells with H2O2 induced apoptosis that was prevented by pre-treatment with catalase, an enzyme that catalyzes the decomposition of H2O2 [87]. A common link between both ROS and apoptosis is TNF-a [88]. Stimulation of the TNF-a receptor leads to the activation of caspase-8, which leads to apoptosis. Cytokines such as TNF-a are known to trigger ROS production, which acts as a mediator of many cellular responses including apoptosis [89], transcriptional factor activation [90], calcium spark activation [91], and insulin signaling [92]. ROS is believed to oxidize mitochondrial pores leading to the release of cytochrome c, a key signal in apoptosis [93]. The link between ROS and apoptosis is clear, however the role particulates have in both of these pathways is still under investigation. Progress has been made to understand the connection, but the focus has been on micron-sized crystalline silica and its role in silicosis. Amorphous silica, which is more relevant to medical applications and to many new occupational exposures, does not

have the same reactive structure of crystalline silica, and therefore further investigation into the causes of silica-induced apoptosis and its link to ROS requires additional careful investigation.

Research Objectives

With the increased production and use of nanoparticles, research into their safety is vital. Currently, there is no clear method to determine organ-specific exposures to adsorbed, inhaled, ingested or injected nanoparticles in their natural state. The technologies that do exist can be labor intensive and may yield only limited information about particle concentrations, sizes, and compositions. Many *in vitro* studies are being performed to assess the safety of particles after inhalation. It is only recently that particle toxicologists have begun to look outside of the lung for tissue damage to other organs. Current research studies are difficult to compare due to experimental variables such as particle composition, or variable assay protocols. Particle exposures have been correlated to increased morbidity and mortality in the population, so the mechanisms by which particles elicit cellular alterations are being avidly investigated. A clear mechanism has yet to be defined.

The studies presented here will describe a technique for the analysis of unlabeled particles, determine cellar responses to particulates, and identify a putative mechanism of particle-induced cellular damage. Chapter 2 addresses the problem regarding the measurement of unlabeled inorganic nanoparticles by using SdFFF in combination with existing methodologies to determine particle concentration, size and composition. Chapter 3 describes a series of cell experiments that compare and contrast vascular, pulmonary and colon cell responses to metal oxide particles. These studies use well defined specific stocks of particles to carry out all experiments to permit direct comparisons of particle types in

different cell lines with minimal variables. Chapter 4 addresses the important question of the mechanism by which particles induce cellular responses by investigating the role of ROS in particle-induced apoptosis. Conclusions from this work are represented in Chapter 5.

CHAPTER 2

A NOVEL METHOD TO DETECT UNLABELED INORGANIC NANOPARTICLES AND SUBMICRON PARTICLES IN TISSUE BY SEDIMENTATION FIELD-FLOW FRACTIONATION

Introduction

In this chapter, a novel methodology to detect unlabeled inorganic nanoparticles will be demonstrated leading to a publication in *Particle and Fibre Toxicology*. This method uses SdFFF technology, as described in Chapter 1, in conjunction with already existing techniques, to detect a mixture of nano-sized (70 nm) and submicron (250 nm) silicon dioxide particles isolated from cell culture and mammalian tissue.

Current nanoparticle research has quantified nanoparticles *in vivo* using some type of unique particle label (fluorescence, radioactivity, or rare elements) to provide important information regarding nanoparticle uptake and translocation. However, most nanomaterials that are commercially produced for industrial and consumer applications do not contain a specific label. Alternatively, unlabeled inorganic nanoparticle amounts have been measured with techniques such as electron microscopy and elemental analysis. However, measuring changes in the concentration of unlabeled particles in tissues with these techniques is difficult. Extracting quantitative information from TEM images is inexact and elemental

analysis does not distinguish particles from soluble forms and provides no information on particle size.

Initial experiments presented in this chapter employed both fluorescence and electron microscopy because of their usefulness in the field of particle toxicology. Although other techniques are shown, this chapter will focus on SdFFF of nanoparticles isolated from mammalian tissue and cell culture via acid and enzyme digestion. The goal of these studies was to precisely identify unlabeled metal oxide nanoparticles and unambiguously distinguish nanoparticles (diameter<100 nm) from both soluble compounds and from larger particles of the same nominal elemental composition. This is an exciting capability that can facilitate epidemiological and toxicological research with natural and manufactured nanomaterials.

Methods

Tissue Preparation

Figure 2.1 outlines the tissue preparation, particle addition and isolation, and particle isolation. Tissue was prepared by collection of whole lungs and livers post-mortem from male Sprague-Dawley rats, in accordance with an IACUC (Institutional Animal Care and Use Committee)-approved protocol. Tissues were snap frozen in liquid nitrogen. The tissues were then ground with a mortar and pestle in liquid nitrogen. The powdered tissue was suspended in 3 ml per gram of tissue of a low-salt buffer (20 mM HEPES, pH 7.9, 25% glycerol, 1.5 mM $MgCl_2$, 0.02 M KCl, 0.2 mM EDTA, 0.2 mM phenylmethylsulfonyl fluoride, and 0.5 mM dithiolthreitol). The tissue was processed by homogenization using a PR0200 series portable homogenizer (ISC BioExpress, Kaysville, UT) at 30,000 rpm until there were no visible chunks and then transferred to a motor-driven Teflon-glass

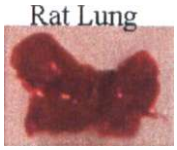

Tissue processing

$N_{2(lq)}$, pulverize
grind and homogenize

2.5 mg 70 nm $Si0_2$
1.25 mg 250 nm $Si0_2$
Incubate 1 hr at RT

Collagenase
Hyaluronidase
Incubate @ 37 °C for 24 hrs

Tissue digestion #1

SDS
Proteinase K
Incubate @ 65 °C for 2 hrs

Tissue digestion #2

Tissue/Particle separation #1
Layer sample over saturated sucrose cushion
and spin 25 min @ 21000 x g

Supernatant:
Low density hydrophilic organics

Phenol Wash

Tissue/Particle separation #2
Spin 25 min @ 21000 xg

Lipids, nucleic acids and other organics

Ethanol

Tissue/Particle separation #3
Spin25min@ 21000xg

Residual phenol

Final sample → **SdFFF**

Figure 2.1 Schematic of the tissue sample preparation protocol. Adapted from Deering *et al.* 2008 [94],

homogenizer (Potter-Elvehjem), (Fisher Scientific) and run at 900 rpm for 2 full passes to ensure the tissue was thoroughly homogenized.

Nanoparticle Addition

Aliquots of particle suspensions in aqueous surfactant (typically 1-2.5 mg) were added to homogenized lung or liver tissue. The addition of particles to homogenized tissue demonstrated nanoparticle detection in a complex mixture of biological material without the complications related to *in vivo* particle distribution, uptake and elimination. Particles were 70 nm diameter SiC>2 (Z-PS-SIL-004-0,07, Postnova Analytics Landsberg, Germany) and 250 nm $Si0_2$ (Alfa Aesar, Ward Hill, MA).

Enzyme Digestion

Collagenase (150 U/ml) and hyaluronidase (100 U/ml) (Sigma Aldrich) were added to the homogenized tissue to break up the extracellular matrix. The mixture was incubated overnight at 37°C with shaking. The particle-spiked tissue was then sonicated using an Ultrasonic Processor (Cole-Parmer, Vernon Hills, Illinois) for 20 seconds (2 second bursts). To hydrolyze proteins, the tissue was incubated with 200 pg/ml Proteinase K (Sigma Aldrich) in 0.5% SDS for 2 hours at 65 °C.

Acid Digestion

A freshly processed lung or liver tissue sample was transferred to a glass test tube and an equal volume of 60% nitric acid (Fisher Scientific) was added. The test tube was placed in a beaker of hot (94°C) water for about 1 hour or until the tissue was completely digested. The samples were then centrifuged and the pellet washed with dilute acid and finally resuspended in 0.1% of the aqueous surfactant FL-70 (Fisher Scientific).

Particle Isolation

The tissue samples were layered over a saturated sucrose cushion and centrifiiged at 21,000 x g for 20 minutes in a microcentrifuge (Eppendorf North America, Westbury, NY). The pellets were resuspended in 0.1% FL-70 and sonicated for 20 sec (2 sec bursts). Phenol was added in a 1:1 (v/v) ratio and incubated with shaking for 5 minutes followed by another round of centrifugation. The pellet was resuspended and washed with 70% ethanol and centrifuged. The final pellet was resuspended 500 pi and sonicated in 0.1% FL-70 with 0.01% sodium azide (Sigma Aldrich, St. Louis, MO).

SdFFF

Analysis of the final samples was performed by our collaborators and Postnova analytics using a Postnova SI01 particle fractionator (Postnova Analytics, Salt Lake City, UT). The injected sample volume was 100 pi using 0.1% FL-70 as the carrier fluid at a rate of 2 ml/minute. The initial speed of centrifugation was 1800 rpm and the final speed was 200 rpm. SdFFF run time was typically 90 minutes. Detection was achieved with a light scattering detector (Brookhaven, Holtsville, NY) at a 90° angle (690 nm laser). Takjiki *et al.* provides further details of the SdFFF methodology [49],

Cell Culture

Human aortic endothelial cells (HAEC, Cambrex, Bio Science Walkersville) were cultured in endothelial cell growth medium-2 (EGM-2, Cambrex, Bio Science Walkersville) at 37 °C, 5% $C0_2$ in a T-25 culture flask (Corning, Corning, NY) or a glass bottom culture dish (MatTek Cultureware, Ashland, MA) until 90% confluent. Cells were treated by replacing the medium with 4 ml of fresh EGM-2 containing 25 pg/cm^2 rhodamine-labeled 70

nm $Si0_2$ (Z-PS-SIL-RFP-0,07 Postnova Analytics Landsberg, Germany) and incubated for 24 hours. To harvest the cells and attached or internalized particles for experiments, the culture medium was removed and the cells were washed with phosphate buffer saline (PBS). Following the removal of PBS, 1ml TrypLE enzyme (Invitrogen) was added according to the manufacturers recommendations. The cells were washed from the dish with fresh media, collected by centrifugation at 200 g, resuspended in 500 pi 0.1% FL-70 (Fisher Scientific) and sonicated with a probe for 20 seconds (2 second bursts). The particles and lysed cell content were then visualized via fluorescence microscopy and processed by enzyme digestion starting with the Proteinase K step (Figure 2.1).

Confocal Microscopy

HAECs were plated at 10,000 cells/cm^2 and grown on a glass bottom culture dish till 80% confluent. The cells were treated with rhodamine-labelled 100 nm $Si0_2$ particles (Z-PS-SIL-RFP-0,10; Postnova Analytics Landsberg, Germany) for 24 hours. The cell membrane was stained with wheat germ agglutinin (WGA) (green) and fixed with ice cold 100% methanol. The treated and stained cells were visualized using an FV300-xy Olympus 1X70 confocal microscope (University of Utah School of Medicine Department of Core Facilities) 60x NA 1.45 oil emersion lens. Images were analyzed using Volocity software (Perkin-Elmer Applied Biosystems, Warrington, UK).

Fluorescence Microscopy

HAECs were plated at 10,000 cells/cm^2 and grown on a glass bottom culture dish till 80% confluent. The cells were treated with rhodamine-labeled 70 nm $Si0_2$ particles (Z-PS-SIL-RFP-0,07; Postnova Analytics Landsberg, Germany) and fixed with ice cold 100%

methanol. The nuclei were stained with DAPI (Molecular Probes, Eugene, OR). The stained cells were visualized using an Olympus 1X50 fluorescent microscope and a Hamamatsu camera. Images were analyzed using ImageJ software.

Transmission Electron Microscopy

Particle samples for TEM were prepared by washing the particles, concentrating them by centrifugation, and resuspending them in high-purity water or by direct collection of the particles from the SdFFF instrument. A 5 pL aliquot was placed on a formvar-coated copper grid and allowed to dry overnight. Samples were imaged on a Philips Techni G2 electron microscope at 100 kV.

Results

The interaction between Si02 nanoparticles and HAECs was evaluated (Figure 2.2). HAECs were treated with 100-nm rhodamine-labeled Si02 particles for 24 hours to permit sufficient interaction between the cells and the particles. To determine the localization of the particles to the cells, WGA was used to stain the plasma membrane. A clear outline of the plasma membrane was not seen due to rapid cycling of the membrane as shown by the control cells stained with WGA in Figure 2.2A. Vesicle formation due to the cycling of the membrane permit visualization of particles colocalized to these vesicles. Figure 2.2C is a z-slice of the circled area in Figure 2.2B. The yellow color observed in this slice demonstrates colocalization of the red particles and the green stained vesicle. Since a primary cell line was used, transfection of a membrane GFP-fusion protein which localizes to the cellular membrane could not be used. With the limitations of fluorescent microscopy, SdFFF was

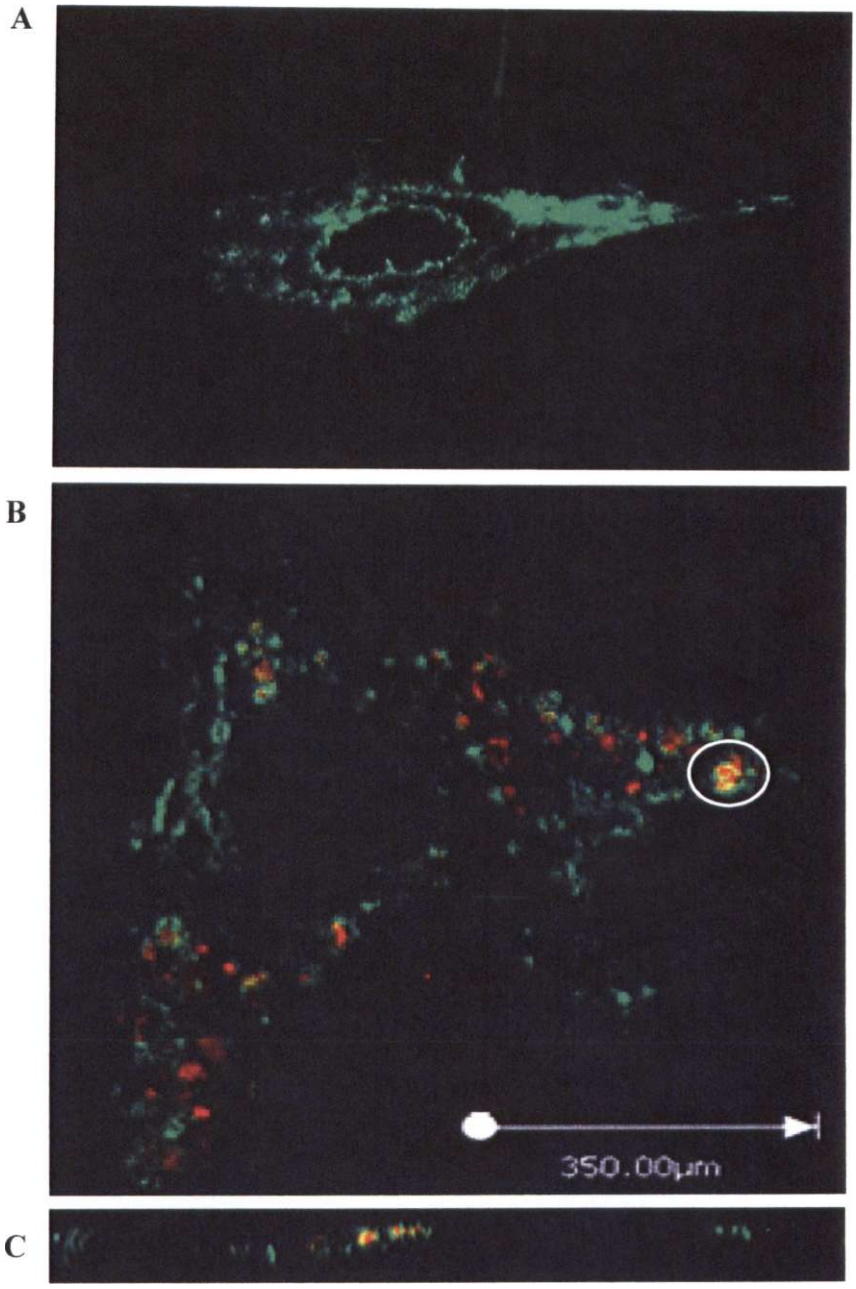

Figure 2.2 Uptake of 100-nm $Si0_2$ into HAECs. A, Confocal microscopy image of untreated control HAECs stained with WGA. B. Confocal microscopy image of HAECs treated with 100-nm rhodamine labeled $Si0_2$ particles (10 pg/cm^2) for 24 hours. C. Z-slice of the circled area in Figure 2.2a showing colocalization of the particles and the WGA. 60X oil emersion lens

used in combination with microscopy to determine uptake of inorganic metal oxide nanoparticles.

Preliminary experiments were conducted to calibrate the instrumentation used in this study, and to determine the amount of particles needed for reliable detection. Dilutions prepared from purchased $Si0_2$ standards (Postnova Analytics) with a known particle size, 70 nm, and a starting concentration of 25 mg/ml of particles suspended in aqueous surfactant were used. With the available light scattering detector, reliable quantification of the standard could be obtained with as few as 7 x 10^{10} particles per injected sample, which is equivalent to 25 pg of particle mass as shown in Figure 2.3. Based on these data, our subsequent experimental work used tissue samples containing 1-2 mg of particles. Using particle aliquots greater than 40 times the limit of detection permitted robust quantification in the experiments that were used to develop nanoparticle recovery protocols.

To compare the SdFFF results to established techniques, fluorescence microscopy and TEM was performed on cell culture samples incubated with rhodamine-labeled Si02 particles for 24 hours, rinsed to remove free floating particle and then prepared by enzyme digestion for FFF analysis. Figure 2.4A shows a TEM image of the starting 70-nm rhodamine-labeled particles in aqueous surfactant, confirming the manufacturer's size. Figure 2.4B demonstrates the interaction of 70-nm rhodamine-labeled particles with HAECs. This image shows localization of the nanoparticles to the cells and formation of micron sized aggregates which are visible by light microscopy. During the first step of our SdFFF particle analysis procedure, the cells were collected, lysed and treated with Proteinase K to digest proteins. Figure 2.4C shows a microscopy image of the cell debris and aggregated fluorescent particles at this stage of the isolation process. A sample removed after the final

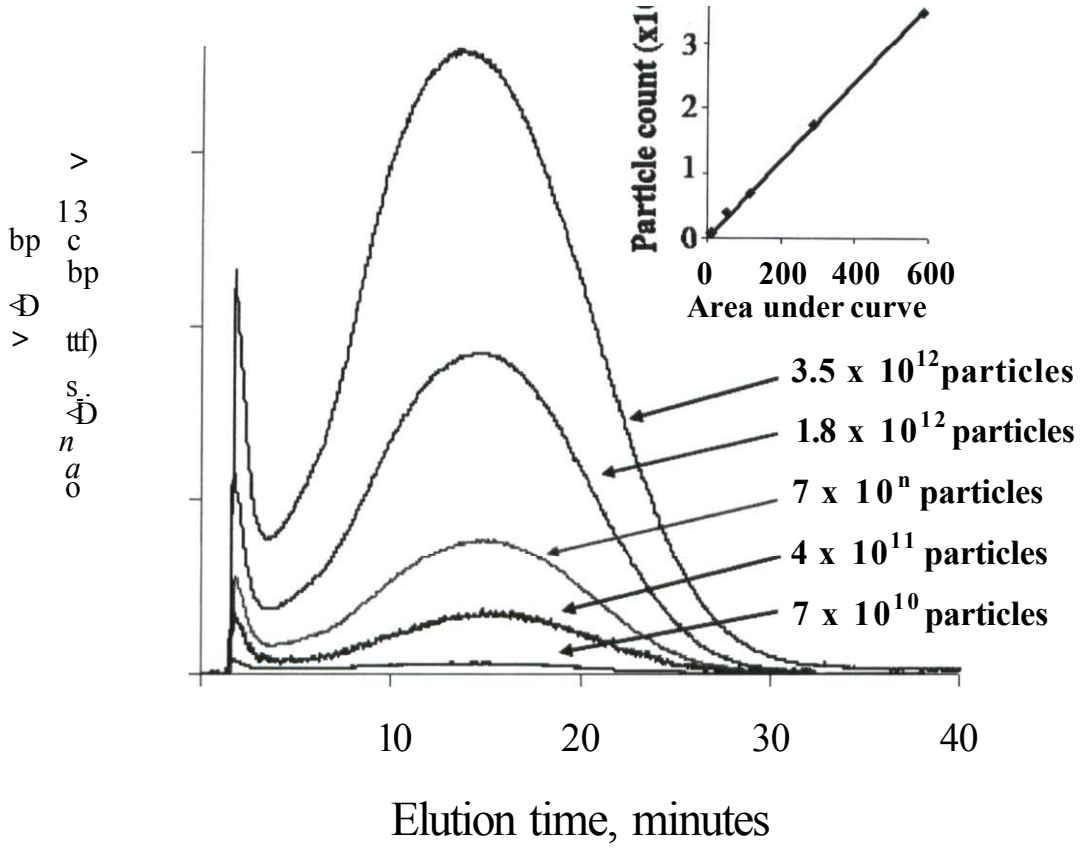

Figure 2.3 Fractograms of 70-nm SiO2 particles injected at different concentrations. Number of particles in each fractogram is shown next to the pointing arrows. The insert shows the calibration curve obtained using the particle number versus fractogram peak area. Adapted with permission from Takjiki *et al.* 2008 [49].

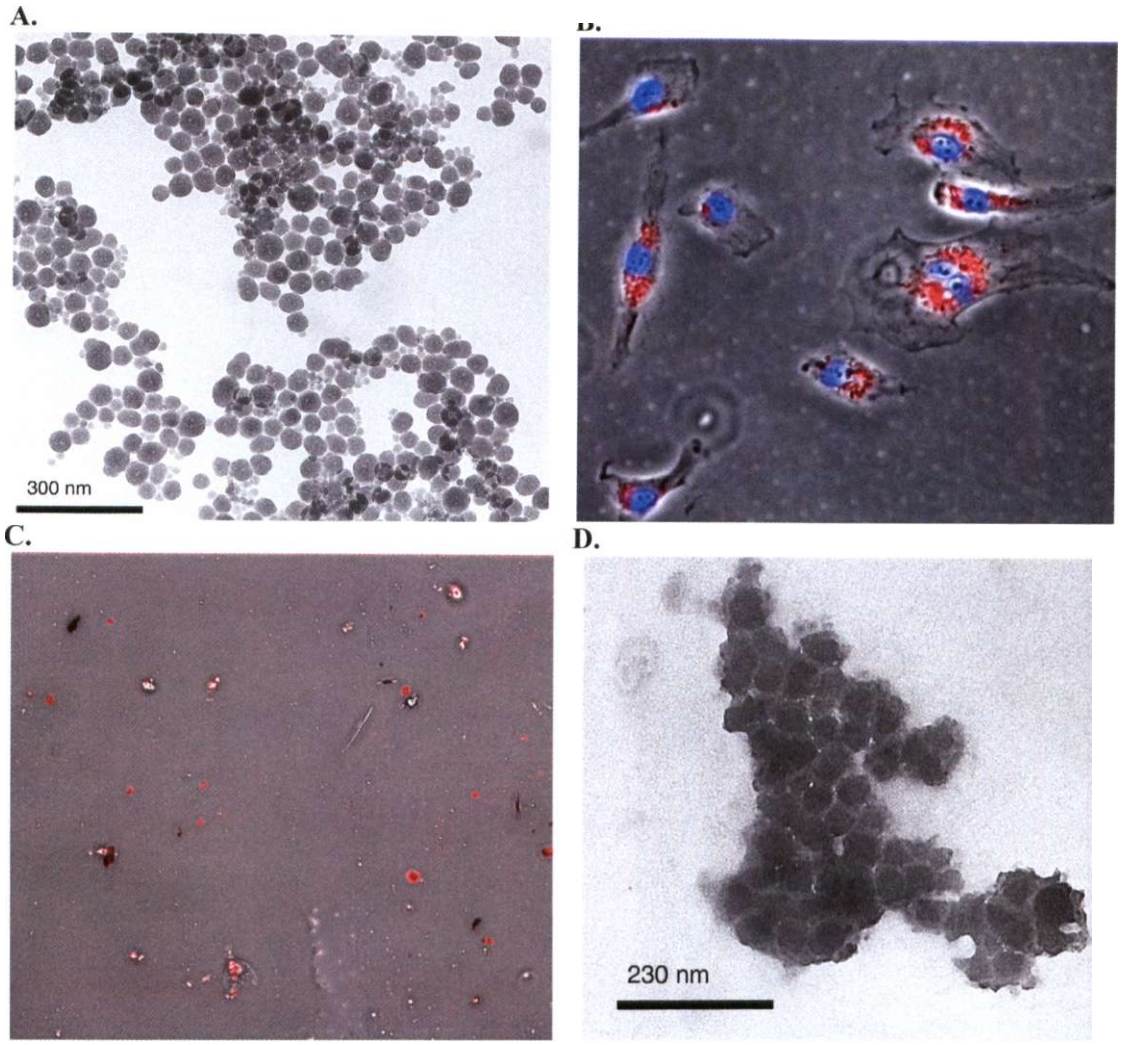

Figure 2.4 Tracking the particles through the isolation procedure. A. TEM image of the stock 70-nm rhodamine-labeled Si02 particles. B. Fluorescence microscopy image of HAECs treated with 70-nm-rhodamine labeled Si02 particles (10 pg/cm") for 24 hours. 20X objective 200X magnification. C. Fluorescent image of cell lysate containing particles. 20X objective 200X magnification. D. TEM image of a dried aliquot of the final sample after cleanup for SdFFF containing 70-nm rhodamine-labeled SiOi particles in dried residual material. Reproduced with permission from Deering *et al.* 2008 [94],

cleanup prior to FFF analysis was analyzed via fluorescence microscopy to demonstrate the power of the cleanup procedure. However, the particles were well dispersed, and not visible by light microscopy (data not shown). Figure 2.4D shows a TEM image of these particles dried onto a grid. The particles are aggregated and coated by residual organic material. SdFFF separation of the particles from the soluble components yields the monodispersed particles that can be seen by TEM (Figure 2.5). These rhodamine-labeled $Si0_2$ particles have the same manufacturer, nominal size, and surface fractionalization as the unlabeled $Si0_2$ particles used for the SdFFF experiments.

Figure 2.6 shows a fractogram demonstrating that unlabeled 70-nm particles could be recovered from acid-digested human lung cells and rat lung tissue, sized by SdFFF, and quantified with a light scattering detector. The elution time (proportional to size) of the particles in the acid-digested sample agreed with the 70-nm standard in surfactant. A "void peak" is commonly seen at the start of an FFF separation [48]. Caldwell *et al.* describe this commonly seen peak as containing soluble components as well as suspended particles small enough to remain uniformly distributed across the channel, even in the presence of the field [43], Since the nitric acid process is limited to acid-insoluble particles, a more gentle tissue processing protocol utilizing protease enzymes was used. Lung tissue was used because it is the primary target in particle inhalation studies. Tissue processing method development experiments (data not shown) led to the protocol described in Methods section, which used specific enzymes to digest the extracellular matrix, included an aqueous surfactant in all processing steps, and used sonication to redisperse the particles after centrifugation.

To demonstrate the capability to distinguish nano-sized (diameter < 100 nm) and submicron particles alone and in lung tissue, mixtures of two different sizes of $Si0_2$ particles

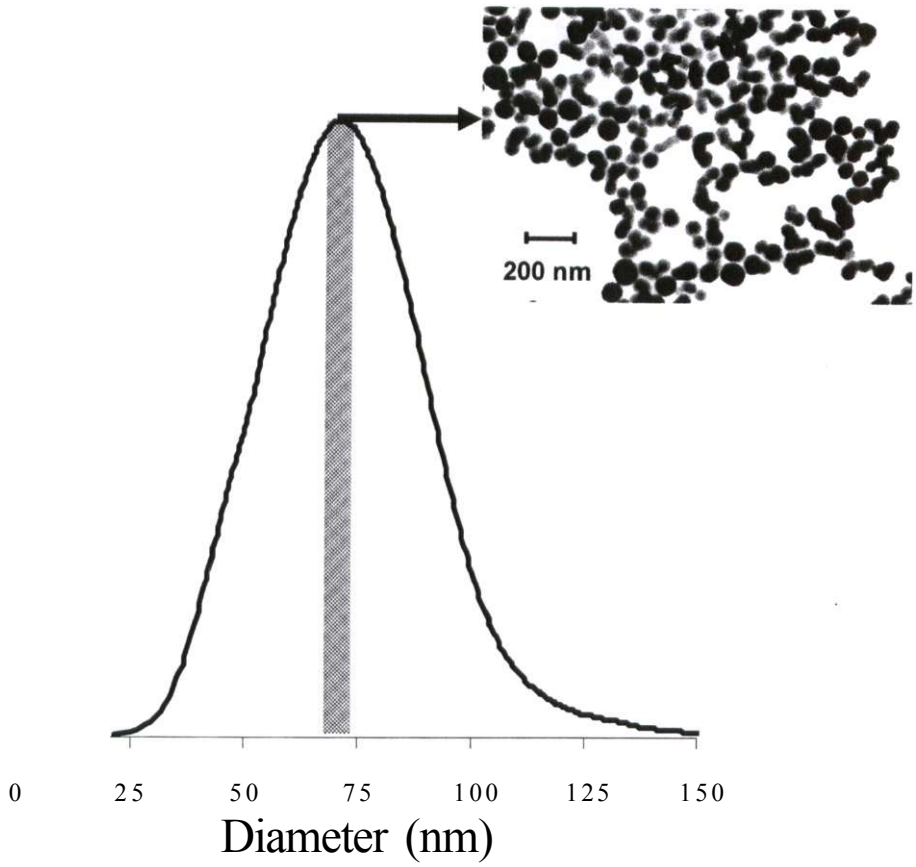

Figure 2.5 SdFFF fractogram of 70-nm SiO_2 nanoparticles extracted from lung cells. The inserted picture is a TEM micrograph of the fraction collected from the peak maximum. Adapted with permission from Takjiki *et al.* 2008 [49].

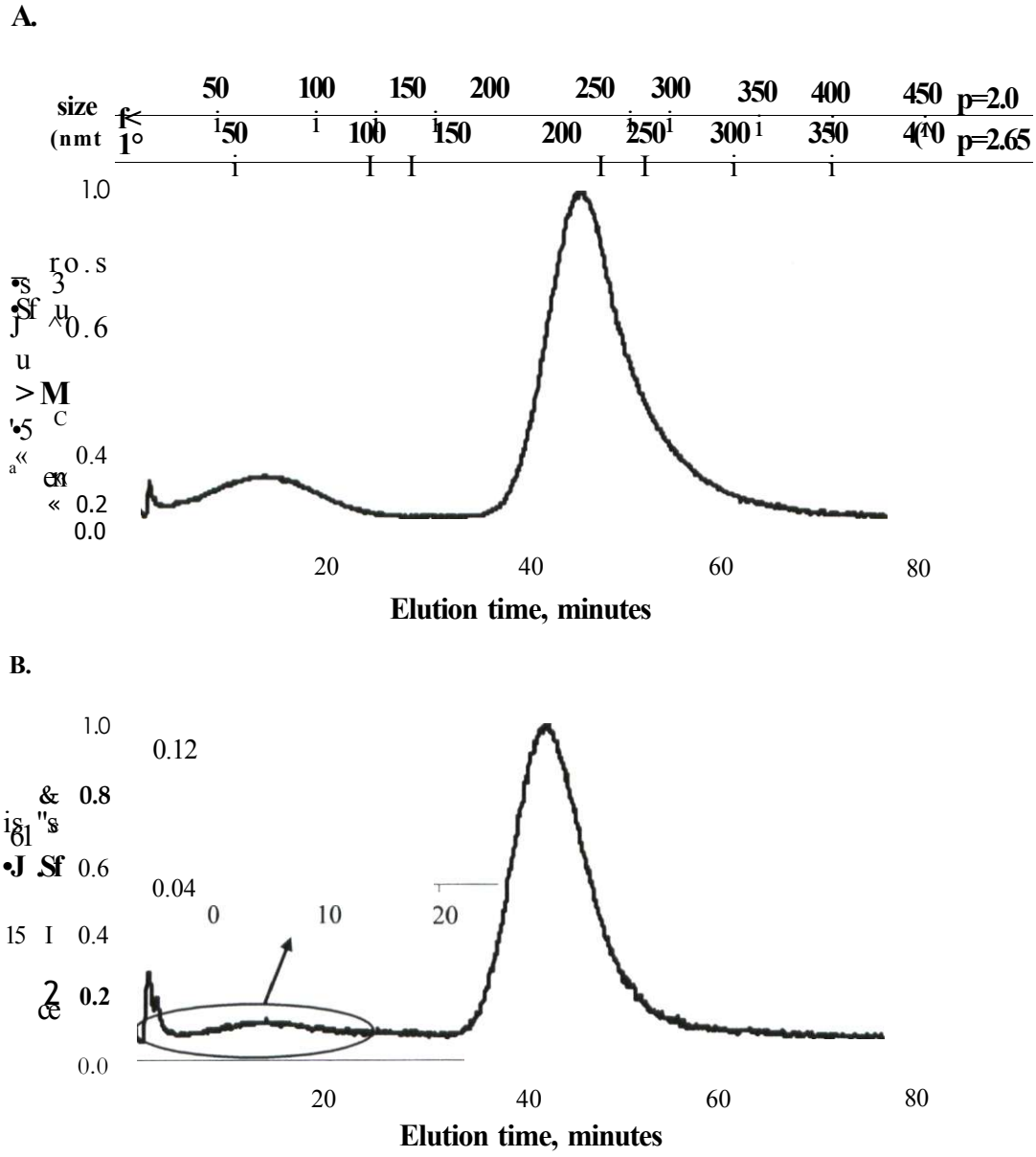

Figure 2.6 Bimodal distribution of 70 and 250-nm particles. A. SdFFF fractogram of the reference sample of 70 and 250-nm particles mixed in surfactant. The secondary x-axis depicts the theoretical particle size corresponding to the elution time for two particle densities. B. SdFFF fractogram of 70 and 250 nm particles isolated from homogenized rat lung tissue. The inset graph is the circled area enlarged, emphasizing the 70 nm particle peak. Reproduced with permission from Deering *et al.* 2008 [94],

were added either to aqueous surfactant (reference sample) or to homogenized lung tissue, which was processed by the tissue digestion procedure. Figure 2.6A shows light scattering versus time from FFF analysis of the reference sample normalized to the largest peak. This sample contains the 70- and 250-nm manufactured SiO_2 particles at a 2:1 mass ratio in aqueous surfactant. Figure 2.6B shows the enzyme-digested rat lung tissue containing 70- and 250-nm manufactured SiO_2 particles at the same concentration as in the reference sample (2:1 ratio). The inset graph is a magnified version of the circled area showing that two particle sizes were clearly detected in a tissue sample. The graphs in Figure 2.6A and 2.6B show the expected bimodal distribution of SiO_2 particles. The difference in the relative sizes of the 70- and 250-nm peaks in the reference samples is due to the size-dependent sensitivity of the light scattering detector. Rayleigh scattering theory predicts that scattering intensity from a single particle varies with d_p^6 where d_p is particle geometric diameter. However, the number of particles for a given mass increases inversely with d_p^3, and the mass ratio of the 70 to 250 nm particles was 2:1. Thus, the expected ratio of peak areas would be about 23:1. A similar experiment using a mixture of 80-nm and 500-nm particles in enzyme-digested rat lung tissue also produced the expected bimodal fractogram (data not shown). The geometrical size of the 70-nm particles was confirmed by TEM of a sample collected after the FFF separation (Figure 2.5).

Well established FFF theory [41] permits the particle size corresponding to a given elution time to be calculated directly from first principles [49]. The calculation is based on measurable physical parameters of the apparatus, the carrier fluid, and the particle density, and involves the equations for settling velocity, particle diffusion rate, and laminar flow profile. Figure 2.6 shows the theoretical particle sizes (top x-axis labels), corresponding to

the measured elution time (bottom x-axis labels), for two different particle densities. These assumed densities, 2.65 and 2.0 g/cm^3, correspond to quartz and the density of the 70-nm particles obtained from the vendor datasheet. These densities span a reasonable range for various amorphous and crystalline forms of $Si0_2$. As can be seen from the differences between the two sets of theoretical sizes, the particle size corresponding to a given elution time does not change dramatically with moderate differences in density. Thus, nanoparticles can be distinguished from micron-sized particles even when the particle composition and density are uncertain.

Particle recovery for the experiment in Figure 2.6A and 2.6B can be estimated from the integrated area under the curve for the SdFFF analysis of the tissue sample and the reference sample. Particle recovery in the enzyme digestion rat tissue processing was 30% for the 250 nm particles and 22% for the 70 nm particles. These recoveries are representative of one set of experimental data.

Discussion

The goal of this study was to develop a technique that compliments existing methodologies and to provide detailed information on the size distribution of unlabeled submicron and nano-sized inorganic particles in toxicology samples. Elemental analysis and radioactive-labeled particles provide mass concentration data but not size data. Microscopy-based techniques, as shown in Figures 2.2, 2.4 and 2.5, provide size data only after image analysis of a sufficient sample to get accurate statistics and intracellular localization if membrane dyes are available for the cell type. Manual image analysis is labor intensive and automated image analysis is subject to artifacts from overlapping particles or poor contrast

from the background. SdFFF complements the available techniques by providing detailed size without requirements for particle labels.

A wide range of unlabeled submicron and nano-sized particles of inorganic materials can potentially be detected in tissue samples by this methodology. All these proof-of-concept experiments used $Si0_2$ particles, but the technique is directly applicable to a much wider range of particle types, sizes, and shapes. The requirements for particle detection by this technique are as follows: the particle must be sufficiently dense compared to the carrier fluid; the particle must have a different index of refraction from the carrier fluid; and the particle must be resistant to the reagents used for tissue digestion and sample cleanup. These requirements are met by essentially all inorganic oxides, pure metal, and elemental carbon-based particle types. Nonspherical particles can also be separated using SdFFF, but mathematical prediction of retention time is more complicated than for spheres. A study using rod-shaped aggregates of latex particles showed that the SdFFF separation time is determined by the maximum dimension of the particle rather than by an average size [95], Thus, this robust methodology is suitable for use in a wide range of particle toxicology studies that involve correlating biological effects with the concentration of nanoparticles in target organs. The particle size distribution information furnished by SdFFF separation will be uniquely applicable to comparisons of the biological effects of solid particles versus the effects of soluble species, a question that cannot be answered by elemental analysis of ashed or acid-digested samples.

The important question of quantifying human lung burden of combustion-generated nanoparticles provides an example of how the sample preparation and SdFFF separation techniques can be used to complement other methods. Vehicle tailpipe emissions contain

submicron particles of carbonaceous material from incomplete combustion and metal oxides from fuel and lubricant additives and engine wear. The carbonaceous primary particulate includes both low-volatility compounds, referred to as organic carbon, and essentially non-volatile large polycyclic molecules, referred to as elemental carbon or black carbon. Grigg *et al.* conducted a study that used light microscopy to measure black material in lung macrophages of healthy children and correlated this lung burden with lung function and modeled levels of particulate matter [96], The light microscopy measured the two-dimensional projected area of particle aggregates. This approach is labor intensive, introduces artifacts from the image analysis, and provides no information on the primary particle size distribution or the composition of the opaque material. Saxena *et al.* recently published a technique for quantitative estimation of diesel and carbon black particles in lung cells based on adapting the thermal-optical-transmittance analytical technique developed for measuring organic and elemental carbon in air pollution samples [97]. This technique provides quantification of the low-volatility and nonvolatile carbon by a precise instrumental analysis method, but again provides no information on the primary particle size distribution or on the metal oxide components. In contrast, SdFFF analysis of tissue provides quantitative information on the particle size distribution after dispersal of the recovered particles by sonication in surfactant. The tissue processing method described in this chapter has the potential of offering high sensitivity since the centrifugation steps concentrate the particles from large volume of digested tissue into a small aliquot for analysis. Sequential collection of samples during a SdFFF run is a well established technique [48]. The collected samples, which represent concentrated and size-segregated fractions of the initial particles, can be further analyzed by transmission electron microscopy or elemental analysis.

Compared to the other approaches cited above, the tissue digestion and SdFFF approach presented here provides the ability to analyze particle size distribution in large samples, such as a whole lung, and provides information on both carbonaceous and metal oxide particles. Carbonaceous combustion particles have lower density than the silicon dioxide used in this study, but analysis of carbon black by SdFFF has been demonstrated [98, 99]. . With additional method development, this technique can become a useful tool to study environmental particle burdens in lungs. Little is known about the background level of naturally formed nanoparticles, and this technique can also be applied to ecosystem studies of sentinel and food chain organisms.

Considerable future research will be needed to fully realize the potential of this technique for nanoparticle characterization in toxicology studies. Specifically, improvements are needed to reduce particle losses during the enzyme digestion and particle recovery steps of the tissue processing, to make the method sufficiently reproducible, and to permit precise quantification of the nanoparticle burden per weight of original tissue. This chapter describes experiments done with relatively high concentrations of the particles because the goal was to demonstrate proof-of-concept. The limit of detection for 70 nm SiC>2 particles was 25 pg of particles per SdFFF analysis sample using a light scattering detector. This particle concentration in tissue is within the range reported by *in vitro* and *in vivo* nanoparticle toxicity studies. For example, a study of fine and nanoscale quartz particles reported statistically significant responses with an intratracheal instillation dose of 1 mg/kg which equated to an initial burden of about 140 pg of particles per lung [100]. In an inhalation study exposing mice, rats, and hamsters to ultrafine $Ti0_2$, the particle burden in the lung was 1.6 mg $Ti0_2$/g of tissue immediately post exposure [101]. Thus, the currently demonstrated

enzyme digestion and FFF detection methodology is applicable to nanoparticle toxicology studies that use superphysiological doses. However, improvement in the method sensitivity will be needed for use in toxicology studies that use environmentally relevant levels of exposures to particulates. The tissue processing protocol involves particle recovery by centrifugation and the centrifugation process intrinsically allows a sample to be concentrated. Processing larger initial tissue samples and recovering the particles in a small final volume is a straightforward way to achieve detection of low particle concentrations in tissue.

Acknowled gements

I would like the thank Postnova Analytics USA and Shoeleh Assemi for technical assistance and sample analysis, and Nancy Chandler at the Health Sciences Center Electron Microscopy Core, who provided the TEM imaging resources.

CHAPTER 3

DIFFERENT VASCULAR AND PULMONARY CELL ADVERSE CYTOKINE RESPONSES TO METAL OXIDE NANOPARTICLES

Introduction

In Chapter 1, the interaction between HAECs grown in a culture flask and 70-nm Si02 at a dose of 10 pg/cm^2 was shown with fluorescence microscopy. At this dose, the particles were clearly interacting with the cells, which appeared intact and alive. This chapter focuses on the effects of metal oxide particles, including silica, on various cell types. Similar studies have been done by Veranth *et al.,* but the focus was on human bronchial epithelial cells (BEAS-2B) treated with a large matrix of particles [102]. Common endpoints included cytotoxicity and cytokine production and release.

Investigation of the cytokine inducing effects of particles has been a staple for determining safety of particles in biological systems. For example, CRP, an acute phase protein clinically used to determine cardiovascular risk, is an indicator of infection, injury and inflammation [103, 104]. CRP detected in the blood is produced from hepatocytes under the transcriptional regulation of IL-6. The increased production and release of IL-6 in any tissue may spill over into systemic circulation, interacting with vascular endothelial cells, leading to activation of transcription factors that change gene regulation [105]. Particle-

induced tissue inflammation may damage the cells at the surface of the tissue, resulting in the loss of integrity of the tissue's defenses [106],

The goal of the chapter is to show that vascular cells are more sensitive to metal oxide nanoparticles than pulmonary cells, causing enhanced cell death and release of cytokines. Direct comparisons between already published research are difficult because of experimental variables. Experimental techniques, cell lines, and particle variability (from manufacturer to manufacturer and from lot to lot), vary among multiple laboratories. Results presented here overcome these experimental variables by using a single source of particles for the treatment and comparing the responses in vascular, pulmonary and colon cell lines directly.

Methods

Cell Culture

Table 3.1 describes the cells used in this study. Human umbilical vein endothelial cells (HUVECs) and HAECs were purchased from Cambrex (Cambrex Bio Science Walkersville, MD) and cultured in endothelial growth medium-2 (Clonetics/Lonza, Walkersville, MD) using passages 4-9, as per manufacturers' recommendations. BEAS-2B cells (CRL-9609) were purchased from American Type Culture Collection (ATCC; Rockville, MD) and cultured in serum-free LHC-9 media, prepared by fortifying Lechner and LaVeck LHC-8 media (BioSource, Camarillo, CA) with retinoic acid (33 nM) and epinephrine (2.75 pM). Normal human bronchial epithelial (NHBE) cells, a primary bronchial epithelial cell line, were purchased from ATCC and cultured in serum-free bronchial epithelial growth media (Clonetics/Lonza, Walkersville, MD), using passages 4-9. Culture flasks (Corning, Corning, NY) for the NHBE cells were precoated at 37°C with

Table 3.1 Cell types used in this study.

Origin	Abbreviation	Definition
Vascular	HUVEC* HAEC*	Human Umbilical Vein Endothelial Cells Human Aortic Endothelial Cells
Pulmonary	BEAS-2B NHBE*	SV40 Transformed Human Bronchial Epithelial Normal Human Bronchial Epithelial Cells
Colon	RKO CaCo2	Human Colorectal Cancer Cell Human Colonic Carcinoma Cell

* Primary cell lines

LHC-basal medium (BioSource, Camarillo, CA) fortified with collagen (30 pg/ml), fibronectin (10 fag/ml), and BSA (10 pg/ml) (Invitrogen, Carlsbad, CA). Caco-2 and RKO, colon cancer cells, were purchased from American Type Culture Collection (ATCC, Rockville, MD) and cultured in Advanced Dulbecco's Modified Eagle Medium (DMEM) supplemented with 2% FBS and Glutamax (Invitrogen, Carlsbad, CA). All cells were maintained at 37°C in an air-ventilated and humidified incubator with 5% carbon dioxide. For subculturing, cells were trypsin-dissociated and passaged every 2-4 days.

Particle Treatment

The particles used in this study are described in Table 3.2. Particles were sterilized with 70% ethanol and dried at 80°C to avoid biological contamination of the cell culture media. Each experiment included an untreated control. Results were replicated using additional independent passages of cells. To limit experimental variability, stock solutions of all materials were made for subsequent experiments. Before treatment of cells, the particles were dispersed by sonication for 5 minutes in an ultrasonic bath, and vortexed immediately before use.

Cell Viability - Dojindo CCK-8 Assay

To measure cell viability, cells were subcultured in 96 or 48-well plates, grown until the cells reached 80% confluence, and incubated with particles for 24 hours. Cytotoxicity of the metal oxide nanoparticles was measured using the Cell Counting Kit -8 assay (Cell Counting Kit CCK-8, Dojindo Laboratories, Gaithersberg MD). This assay measures metabolic activity by mitochondrial reduction of the reagent to form a colored product, and results were adjusted by subtracting the response of the blanks, and reported as fold over

Table 3.2 Metal oxide particles used in this study.

Particle Defined

Full Name	Formula	Nano	Micron
Cerium IV Oxide	CeO_2	9-15 nm[a]	5 pm[a]
Iron (III) Oxide	Fe_2O_3	*i* [a] 3 nm	5 pm[a]
Silicon Dioxide	SiO_2	10 nm[b]	0.5-10 pm[c]
Titanium Dioxide	TiO_2	[c] [b] 5 nm	1-2 pm[a]
Zinc Oxide	ZnO	8-10 nm[a]	44 pm[a]

[a]Alfa Aesar

^anoStructure and Amorphous Materials INC

[0] Sigma Aldrich

untreated control. Immediately after harvesting the media for cytokine analysis, WST-8 reagent was mixed with cell culture media (4%), added to the cells and incubated for 2 hours before reading absorbance. Data were quantified the absorbance ratio (>.=450/630).

Enzyme-Linked Immunosorbent Assay (ELISA)

To measure the cytokine release, cells were plated in 48-well plates, grown until the cells reached 80% confluence, and treated with particles. The media was harvested from the wells 24 hours after particle treatment. The concentration of interleukin-6 (IL-6) in the cell culture media was determined using a sandwich ELISA assay. For IL-6, 96-well Nunc MaxiSorp immuno plates (Fisher Scientific) were coated with anti-human IL-6 (eBioscience; San Diego CA) overnight at RT followed by exposure to the cell culture media. Biotin-conjugated anti-human IL-6 (eBioscience; San Diego CA) was then added to the reaction and detected using avidin horseradish peroxidase (eBioscience, San Diego CA). Absorbance was read on a Molecular Devices Model SpectraMax 250 plate reader with Softmax Pro software. The concentration of IL-6 was determined based on a standard curve, consisting of recombinant human IL-6 standard (R&D systems, Minneapolis, MN) run on each plate.

Real-Time PCR

An overview of the real-time PCR methodology is described in Figure 3.1. Cells were plated at a density of 10,000 cells/cm^2 and grown in a 6-well plate until 80% confluent and then treated with particles. An additional 100 nm Si02 particle (Z-PS-SIL-RFP-0,1; Postnova Analytics Landsberg, Germany) was used in this study. After 24 hours, unless otherwise specified, total RNA was extracted from treated cells using the RNeasy total RNA isolation kit (Qiagen, Chatsworth, CA). One microgram of total RNA was reverse-

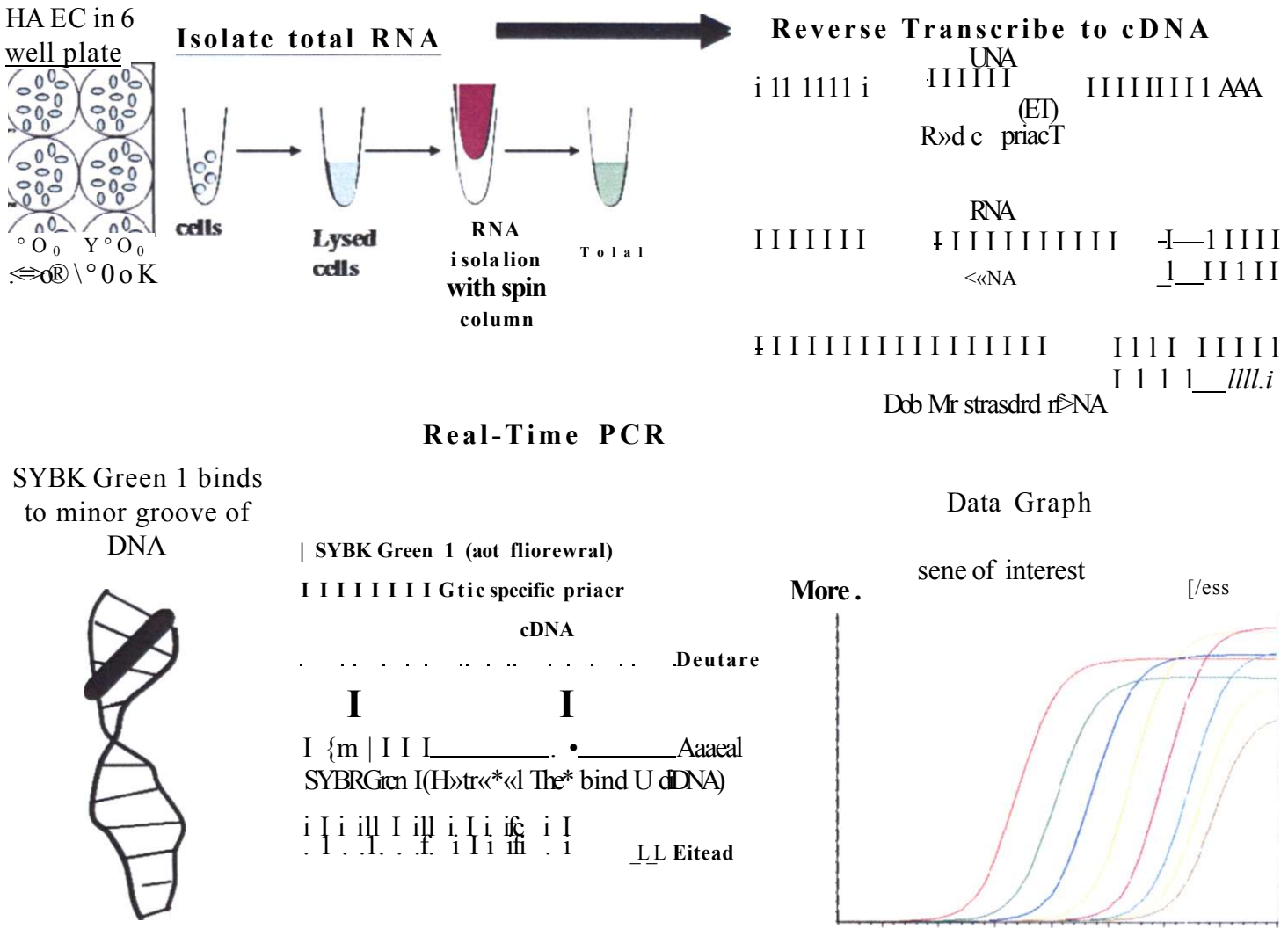

Figure 3.1 Schematic diagram of real-time PCR process.

un

transcribed to cDNA using random hexamer primers and a cDNA synthesis kit containing Superscript II RT enzyme (Invitrogen, Carlsbad, CA). The resulting cDNA was then diluted 1:50 and 2.5 pi used for each real-time PCR reaction. IL-6, IL-8, and 18s rRNA genes were amplified using the following primers: 18s rRNA: Sense- 5'- TGGTTGCAA AGC TGA AAC TTA AAG -3' and anti-sense- 5'- ACT CAA ATT AAG CCG CAG GC -3', IL-6: Sense- 5' AAC CTG AAC CTT CCA AAG ATG G -3' and anti-sense- 5'- TCT GGC TTG TTC CTC ACT ACT -3', IL-8: Sense- 5'- ACT GAG AGT GAT TGA GAG TGG AC -3' and anti-sense 5'- AAC CCT CTG CAC CCA CTT TTC -3'. The real-time PCR reaction was carried out using 4 pM primer, diluted template and LightCycler" 480 SYBR Green I Master Mix (Roche, Indianapolis, IN) using the manufacturers recommendations. The reaction was run on a Lightcycler" 480 system (Roche, Indianapolis, IN). Standard curves were prepared for each gene. IL-6 (Image: 3884652) and IL-8 (Image: 3882471) image clones were purchased from ATCC. (ATCC, Rockville, MD). 18s rRNA was cloned into TOPO 2.1 vector as per manufacturers recommendations (Invitrogen, Carlsbad, CA). The data was analyzed using Lightcycler 480 software (Roche, Indianapolis, IN). The results are reported as fold over control after normalization to the housekeeping gene.

Statistical Analysis

The dose at which 50% of cells are dead (LD_{50}) values were obtained by nonlinear regression analysis using the sigmoidal dose-response (variable slope) equation (Prism 4, GraphPad Software Inc, San Diego, CA). Statistical analysis was performed using either a One- way ANOVA with a Dunnett's post hoc test or a student's *t*-test ($p < 0.05$).

Results

Cytotoxicity of metal oxide particles

Cytotoxicity was measured by incubating the cells listed in Table 3.1 with metal oxide particles. After a 24 hour incubation, cytotoxicity was assayed by the reduction of the CCK-8 reagent which measures metabolic activity of the mitochondria. Figure 3.2 shows the dose response graphs of HAECs treated with the metal oxide nanoparticles listed in Table 3.2. The bars illustrate fold over control responses, and control values are untreated cells. The dose range is 1.0 to 316 pg/cm^2, common doses used among particle toxicologists in cell culture to elicit cellular responses. Figure 3.2A shows a dose response to 10-nm SiC>2 particles. The lowest dose that produced a statistically significant loss of viability was 31.6 pg/cm . The other metal oxide nanoparticles in Figure 3.2 show a similar dose response, but the exception was ZnO, which results in greater than 90% loss of viability at doses higher than 10 pg/cm .

To compare vascular cell responses to pulmonary epithelial cell responses to particles, BEAS-2B cells were treated with the same batch of particles as shown in Figure 3.3. The lowest dose that produced a statistically significant loss of cellular viability with BEAS-2B cells was 100 pg/cm^2. Other nanoparticles did not elicit significant cytotoxicity at the highest dose tested. ZnO caused complete cell death at concentrations higher than 3.16 pg/cm .

A full comparison of the LD50 of metal oxide particles in various cell types is summarized in Table 3.3. Some of the particles did not elicit cytotoxicities to multiple high concentrations, so LD50 values are simply estimated to be greater than 350 pg/cm . These values are shown as gray highlighted boxes in Table 3.3. The overall goal of this table is to

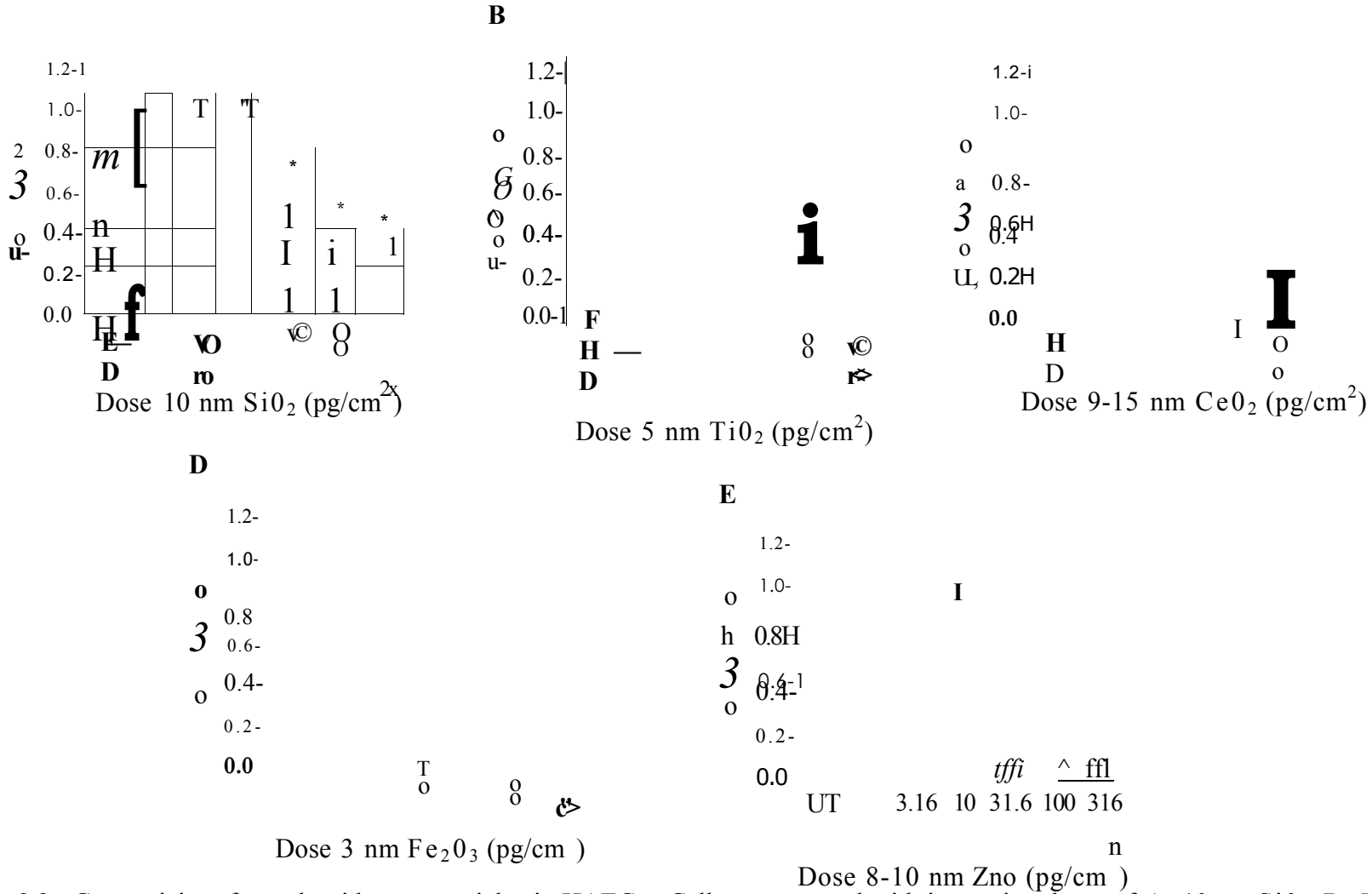

Figure 3.2 Cytotoxicity of metal oxide nanoparticles in HAECs. Cells were treated with increasing doses of A. 10 nm SiO_2 B. 5 nm Ti02 C. 9-15 nm CeO_2 D. 3 nm Fe_2O3 E. 8-10 nm ZnO. Data represent viability represented as fold over untreated control. Each bar represents n=6. Statistically significant decrease in cell viability relative to untreated controls (One-way ANOVA, Dunnett's post hoc test, $p<0.05$) are identified with an asterisk (*).

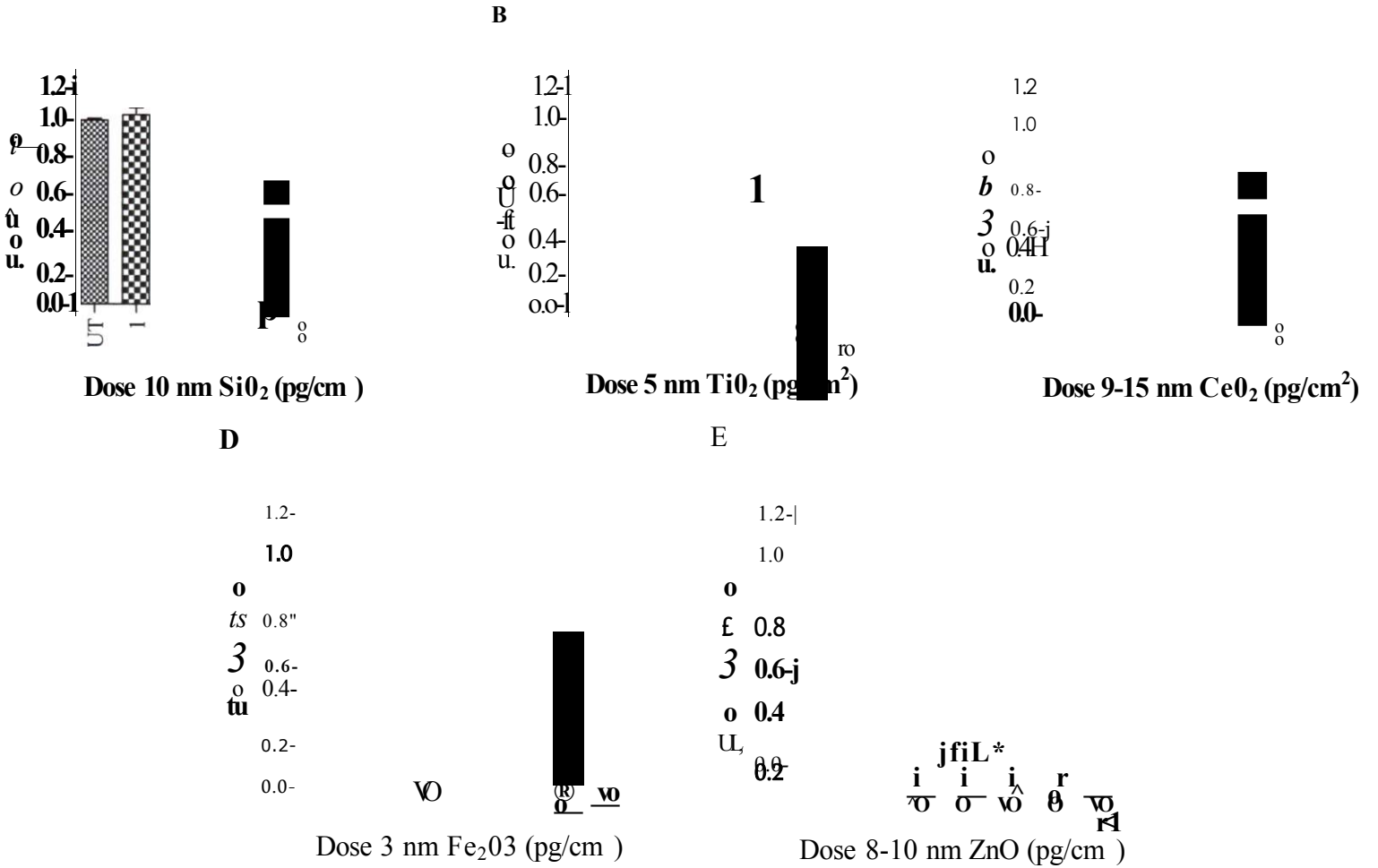

Figure 3.3 Cytotoxicity of metal oxide nanoparticles to BEAS-2B cells. Cells were treated with increasing doses of A. 10 nm SiO_2 B. 5 nm TiO_2 C. 9-15 nm CeO_2 D. 3 nm $Fe_2C>3$ E. 8-10 nm ZnO Bars show viability as fold over untreated control. Each bar represents n=6. Statistically significant decrease in cell viability relative to untreated controls (One-way ANOVA, Dunnett's post hoc test, $p<0.05$) are identified with an asterisk (*).

Table 3.3 LD50 (pg/cm^2) of metal oxide nanoparticles treated cells.

	NANO					MICRON				
	$Ce0_2$	**Fe_20_3**	**SiO_z**	**$Ti0_2$**	**ZnO**	**$Ce0_2$**	**Fe_20_3**	**$Si0_2$**	**$Ti0_2$**	**ZnO**
HUVEC	40	33	60	37	26	34	89	37	35	13
HAEC	19	11	29	19	12	30	65	35	100	10
BEAS-2B	153	53	**>350**	**>350**	8	**>350**	**>350**	**>350**	**>350**	8
NHBE	**>350**	**>350**	**>350**	146	4	**30**	**>350**	**>350**	**>350**	1
RKO	143	**>350**	**>350**	**>350**	21	**>350**	**>350**	129	**>350**	21
CaCo2	63	**>350**	**>350**	**>350**	30	**>350**	**>350**	**>350**	105	22

demonstrate that the vascular cell lines treated with metal oxide particles have lower LD50 values than the pulmonary and colon cell lines. Micron-sized particles were also tested to determine if this overall sensitivity was selective for nanoparticles. The LD50 values were generally higher with micron-sized particles, but the overall enhanced sensitivity of vascular cells is still observed.

Cytokine Response to Metal Oxide Nanoparticles

To ensure that the enhanced sensitivity of vascular cells applies to additional adverse effects, cytokine responses to metal oxide nanoparticles were measured. An ELISA was used to measure IL-6 concentrations in the culture medium harvested from cells after a 24 hour exposure to nanoparticles. The results of HAECs treated with titanium, cerium and silica nanoparticles are shown in Figure 3.4. All of the particles tested show positive dose-response and reach statistical significance. Statistically significant IL-6 response was seen at doses as low as 0.1 pg/cm^2 with Si02 (Data not shown) which is near a calculated physiologically relevant dose for injected nanoparticles used for drug delivery or imaging contrast agents [51].

NHBE cells, a primary bronchial epithelial cell line, shows no significant increase in IL-6 release even at doses previously shown to be cytotoxic, Figure 3.5. IL-6 release, although not significantly produced in these studies was shown to be induced by soluble vanadium during previous studies in the Veranth Lab at the University of Utah. A comparison of the cytokine inducing dose of the metal oxide particle for the different cell types is shown in Table 3.4. Micron and nano-sized particles are shown, and again the most important difference is observed between the cell types, not the particle sizes. The data in this table are a work in progress suggesting a pattern of enhanced sensitivity of the vascular

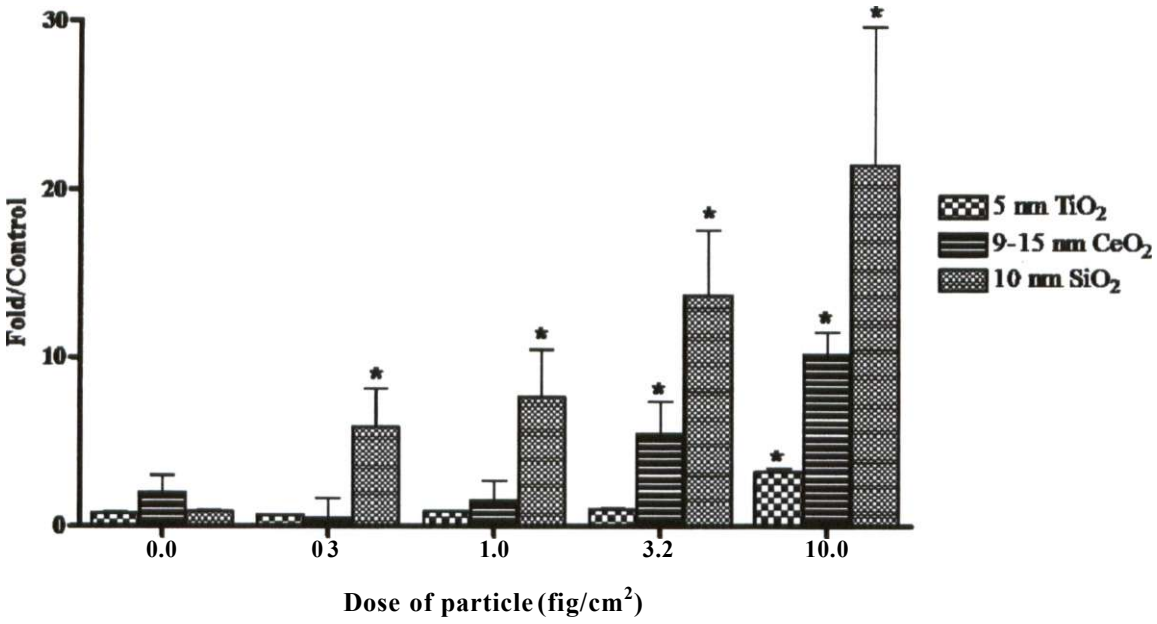

Figure 3.4 IL-6 protein release from HAECs. Bars show IL-6 concentration represented as fold over untreated control. Each bar represents at least n=3. Statistically significant changes in IL-6 relative to untreated controls (student's *t*-test, $p<0.05$) were not observed.

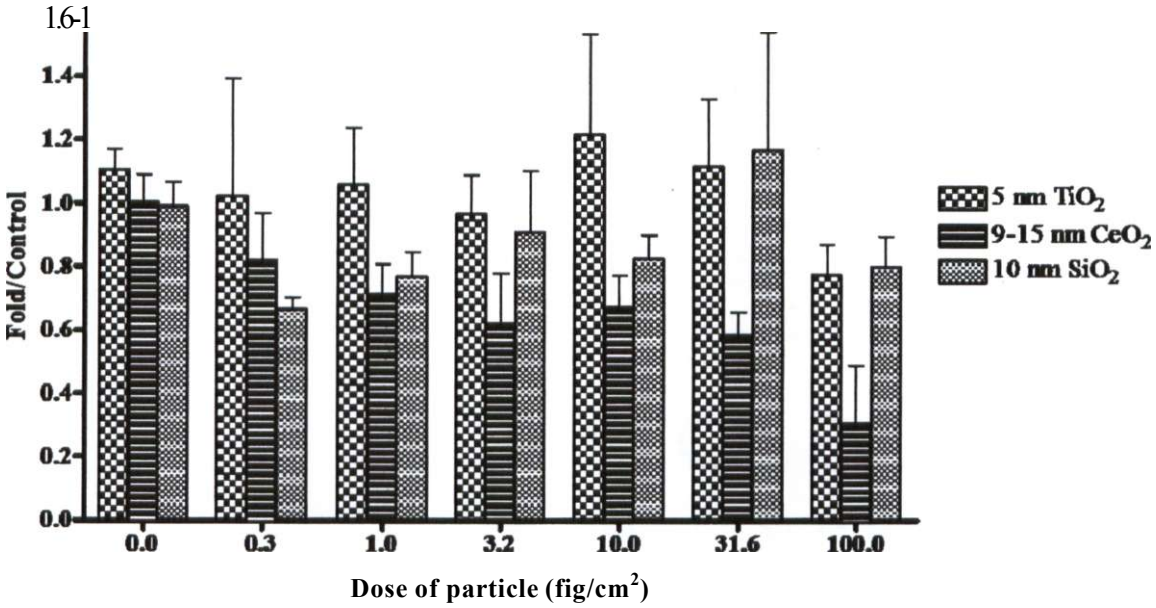

Figure 3.5 IL-6 protein release from NHBEs. Bars show IL-6 concentration represented as fold over untreated control. Each bar represents at least n=3. No statistically significant increases in IL-6 relative to untreated controls were observed.

Table 3.4 Concentration resulting in statistically significant IL-6 production (pg/cm^2)

	NANO				MICRON			
	$Ce0_2$	**$Si0_2$**	**$Ti0_2$**	**ZnO**	**$Ce0_2$**	**$Si0_2$**	**$Ti0_2$**	**ZnO**
HAEC	3	0.1	10	*	3	0.3	0.3	*
NHBE	>100	>100	>100	*	no data	100	100	no data
CaCo2	no data	>100	>100	100	no data	no data	no data	no data

* significant cell death a low concentrations

cells however further experiments with a larger matrix of cell types is needed.

To confirm the cytokine effects of metal oxide nanoparticles to HAECs, quantitative real-time PCR for IL-6 and IL-8 message was performed. An ELISA was performed after a 24 hour treatment, measuring the accumulation of IL-6 protein in the cell culture medium over time. For the measurement of IL-6 and IL-8 mRNA induction, a time course was needed to determine the point at which induction was the greatest. Figure 3.6 graphically shows the time course results for IL-6 and IL-8 and the peak gene induction for both genes occurred at 12 hours or later. IL-8 gene induction appears to be higher in HAEC and HUVECs. The difference between vascular cells depends on the gene. For IL-6 HAEC seem to have a higher response and the opposite is true for IL-8. The gene induction for both IL-6 and IL-8 persists to 24 hours (data not shown). A time course was not performed for pulmonary cells considering the results of the IL-6 ELISA showed no increase in cytokine production over 24 hours when treated with particles. Figure 3.7 shows a lack of cytokine gene induction in NHBE cells at 24 hours at two doses.

Discussion

The goal of this chapter was to show that vascular cells, represented as HAEC and HUVECs, are more sensitive to metal oxide nanoparticles than other cell types including pulmonary and colon cells. The primary focus of previous research has been on environmental and occupational exposures to particles. Two of the most common routes of entry of these particles are through inhalation and ingestion. Therefore, pulmonary cells have been a primary focus of study. Recent publications have suggested that nanoparticles translocate into systemic circulation, allowing interaction with other tissues

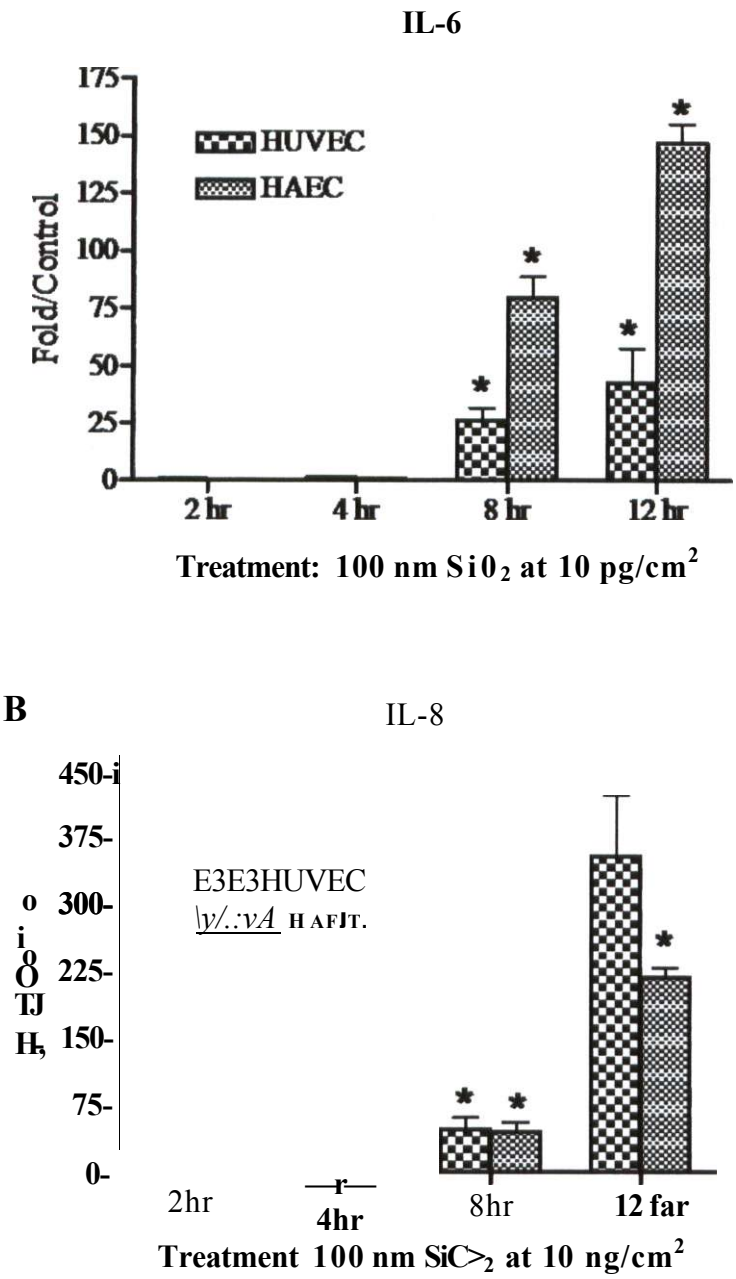

Figure 3.6 Cytokine gene induction in vascular cells. A. IL-6 gene induction in HAEC and HUVECs treated at 2, 4, 8, and 12 hour time points with 100-nm $Si0_2$. B. IL-8 gene induction. The dose used was 10 pg/cm , a dose which does not cause significant cytotoxicity. Bars are copies of IL-6 normalized to copies of 18s rRNA and then represented as fold over untreated control. Each bar represents n=3. Statistically significant changes in message relative to untreated controls (student's /-test, $p<0.05$) are identified with an asterisk (*)

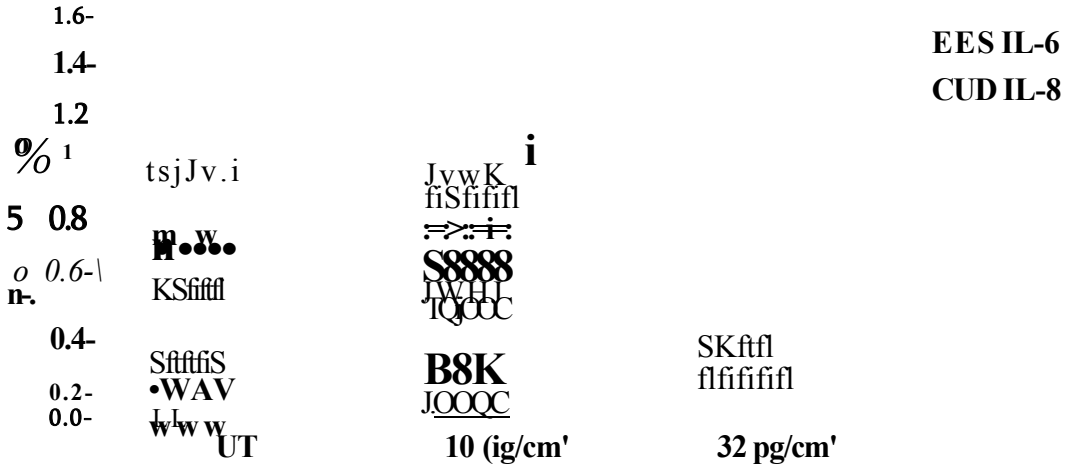

Figure 3.7 The cytokines IL-6 and IL-8 gene induction in NHBEs. RNA was harvested at 24 hours. The doses used were 10 and 31.6 pg/cm^2, which does not cause significant cytotoxicity. Data represents copies of IL-6 or IL-8 gene copies normalized to copies of 18s rRNA and then represented as fold over untreated control. Each bar represents n=3. Statistically significant changes in message relative to untreated controls (student's *t*-test, $p<0.05$) were not observed.

to occur [24, 33-35, 40]. As mentioned in Chapter 2, many particles used to evaluate deposition typically have a specific label, making them of limited relevance to environmental and occupational exposures. Geiser *et al.* tracked unlabeled 22-nm $Ti0_2$ in the lung using energy-filtering transmission electron microscopy, and found particles on the luminal side of airways and alveoli as well as in all major lung tissue compartments, cells and in capillaries [22]. Thus, the relevance of the effects of inhaled nanoparticles in the vasculature becomes apparent due to secondary vascular exposure. Beyond environmental and occupational exposures, nanoparticles are being used for drug delivery, also validating the need for investigation into the effects particles have on the vasculature. Slowing *et al.* provide a review of mesoporous silica nanoparticles used for controlled release drug delivery [107].

The importance of the metal oxide particles used in this chapter was reviewed in Chapter 1. In this Chapter, effects of metal oxide particle on vascular versus pulmonary and colon cells was examined. A careful comparison of susceptibility of multiple cell lines to nanoparticles has not been reported. Some studies have been done in various cell lines by different research groups using an array of particles. However, comparisons of these experiments are difficult because different experimental conditions were used. Particle variability is a major confounding variable not only from manufacturer to manufacturer, but from lot to lot from the same company. Veranth *et al.* described the effects of culture medium, culture well size, percent confluence and source of cell types as major factors in measurements of cellular responses to particles, demonstrating the need for a uniform experimental matrix as described in this chapter [108].

The data shown in this chapter indicate that vascular endothelial cells are more sensitive to metal oxide particles than pulmonary and colon cell lines. However, some

cytotoxicity reports in vascular cells do not corroborate these results. Peters *et al.* treated microvascular endothelial cells with $Ti0_2$ and SiC>2, showing no loss in viability and a slight increase in IL-8 protein release [109]. This difference or lack of sensitivity is most likely due to the cell type differences, since microvascular cells express different proteins, are responsible for different cellular functions, and are under different stresses than HAECs and HUVECs. A study using ZnO and Fe203 was done in HAEC showing that these particles are cytotoxic and induce IL-8 message, with a maximum effect at 4 hours [110]. These data agreed with our results for zinc and iron oxide except the maximum induction we observed was at 12 hours. Fujii *et al.* treated primary human bronchial epithelial cells that they isolated from donor lungs with PMio showing maximum IL-8 induction at 8 hours [62]. These results may disagree because of the differences between experimental techniques. The cells treated for PCR in this chapter were done in a 6 well plate. The settling velocity of the particle as described in Chapter 1 may alter the actual concentration at a specific time point. Additional variables might include experiments with different volumes, with particles of varying densities. The cells may have come from a different donor/vendor, altering the cells response to the particles. Additionally, as shown in precious studies, responses can be titrated by using different culturing conditions [108]. Chang *et al.* suggest that Si02 toxicity is based on metabolic activity of the cell type, and that cells with a longer proliferation time are more sensitive to silica [111]. Further research will need to be done to determine the cause of these differences.

Gojova *et al.* also showed the same complete cell death with ZnO at doses of 50 pg/ml which is roughly equivalent to our 31.6 pg/cm^2 dose [110]. Follow up work by the same group showed that the effects were not from liberated metal ions [110]. These data

were confirmed by the Moos lab at the University of Utah indicating it is the particles causing the observed affects. The mechanism by which the particles elicit tfiis effect is still under investigation. Perhaps particles binding to surface receptors is occurring or the particles are internalized, activating signaling cascades, leading to cell death.

Incubations of particles with colon cells, though relevant due to ingestion of nanoparticles, are rarely published. However, since the colon is constantly exposed to various contaminants from food and other ingested materials, and serves as a barrier to the rest of the organs of the body, it is not surprising that the particles used in this study did not cause significant toxicities or inflammation. Translocation of nanoparticles may occur through the colon since it is a site of nutritional absorption. The pulmonary cells may be subject to the same lack of sensitivity. The lung is also exposed to a large variety of environmental pollutants and may have become desensitized to the toxic effects of particles. Unlike colon cells, with exposure to particles pulmonary cells have been extensively studied. Veranth *et al.,* using the same particles, showed a lack of cytotoxicity and minimal cytokine production in BEAS-2B cells [102], Other research by Steerenburg *et al.* show the same lack of response to $Ti0_2$ particles in BEAS-2B cells but show a pronounced response to fumed silica, which we did not observe [112]. NHBE cells are potentially more important comparison to HAECs. Both of these cell types are primary cultures, not immortalized or cancer derived. All NHBE data presented here indicate that these cells are not sensitive to the metal oxide nanoparticles, results similar to BEAS-2B cells. While the metal oxide particles tested here do not elicit a pronounced effect in the pulmonary cells, some particle types are cytotoxic and induce a cytokine response. In A549 lung cells, Lin *et al.* showed that amorphous silica nanoparticles caused cell death greater than the well characterized

crystalline silica [113]. This does not completely contradict the data shown in this chapter, since a significant loss of viability was shown in pulmonary cells treated with Si02. Fujii *et al.* show that human bronchial epithelial cells exposed to ambient air pollution particles, PMio, show significant IL-8 induction [62],

An interesting unexpected observation was the difference between vascular cell lines. The LD50 values for HUVECs are higher than for HAECs. Furthermore, IL-6 and IL-8 gene induction (Figure 3.6) differs between the cells as well. Both of these cells are subcultured in the same medium in the same manner, the only difference between them is their tissue origin and donor. HAECs are isolated from the aorta and HUVEC are isolated from the umbilical vein. Studies using isolated umbilical cords show that particles do not enter placental circulation [114] which is important because the umbilical cord serves as an important barrier protecting the growing fetus. Differences between aortic and venous cells may be important factor influencing the differences in gene induction and cytotoxicity. The most notable difference between veins and arteries is the blood they both carry. Arteries carry oxygenated blood from the heart to tissues while veins carry deoxygenated blood, CO2 and other waist back to the heart. However, umbilical veins carry oxygenated blood to the growing fetus. Other difference between these cells may be the variation of genes expressed in the different cell types and their capability to produce and detoxify ROS. Viability data from HAECs is pooled from multiple donors with minor variations between the two. Investigation into the mechanism by which particles induce cellular alterations in aortic versus venous cell lines as well as other vascular endothelial derived cells needs to be completed before any conclusions can be made.

A popular hypothesis among particle toxicologists is that surface area or the composition of the particle determines the cellular effects. The cytotoxicity results presented in Table 3.3 do not conclusively support this surface area hypothesis. For instance, the difference in LD50 for SiC>2 in HAEC is no different for nano- (large surface area) versus micron-sized (smaller surface area) particles, both LD50S were approximately 30 pg/cm^2. However, in the same cell type, TiO_2 varies from 19 pg/cm^2 for nano and 100 pg/cm^2 for micron-sized particles. These results may support the theory that the composition of the particle is responsible for the cellular seen, as shown by all results with ZnO. These particles clearly kill all cells equally. As stated previously, free zinc ions are not responsible for cell responses. Each particle of composed of different metal ions may interact with cells differently. This interaction may be internalization or binding to surface receptors.

Future directions for this research should focus on the difference in susceptibilities of the cell types. A gene array of all three cell types treated with nanosilica may give insight into which genes are important in the various cell lines leading to their differential responses. Additionally, studies should be done to determine the mechanism by which particles cause cytokine induction. Studies in the Veranth Lab were performed, pretreating BEAS-2B cells with inhibitors of cytokine receptors as well as inhibitors of the MAP kinase pathway; however results IL-6 ELISA results were inconclusive.

CHAPTER 4

EVALUATE THE ROLE OF APOPTOSIS AND REACTIVE OXYGEN SPECIES IN ENHANCED SUSCEPTIBILITY OF VASCULAR CELLS

Introduction

In previous chapters, experiments have focused on HAECs interaction with and sensitivity to silica particles. In this chapter, the mechanism of this enhanced sensitivity will be investigated through examination of apoptosis and the mechanisms leading to apoptosis.

Knowledge regarding silica-induced cellular apoptosis is increasing daily, and the majority of the studies focus on crystalline silica or Min-U-Sil, typically 1 -5 pm particulates. The study of micron-sized crystalline silica is important because of occupational exposure to silica lead to a well characterized syndrome known as silicosis. The role of silica-induced apoptosis in pulmonary cells after exposure to micron-sized crystalline silica has been thoroughly studied [115-118]. Furthermore, micron-sized crystalline silica-induced apoptosis and ROS have been investigated in HAECs [119].

The goal of this chapter is to show that vascular cells treated with 10-nm amorphous silica stain positive for apoptosis that can be prevented by inhibiting the formation of ROS. To quantify apoptosis, an Annexin V (AV) assay was used. This assay utilizes the externalization of phosphatidylserine (PS), a cell membrane phospholipid, typically found on

the cytoplasmic side of the cell membrane. PS is flipped to the outer membrane of the cell during apoptosis, serving as a signal for recognition and degradation of apoptotic cells by phagocytes. To detect apoptosis, FITC-conjugated AV binds to PS and the fluorescence is measured by flow cytometry. Gating of fluorescent cells permits the quantification of the cells undergoing apoptosis in a given population. Figure 4.1 depicts this process. Additional studies were performed using this assay to assess the role of ROS in silica-induced apoptosis.

Methods

Particles

The particles used in this Chapter include 10-nm (Nanostructured & Amorphous Materials, Inc., Houston, TX) or 70-nm (Z-PS-SIL-004-0,07, Postnova Analytics Landsberg, Germany) Si02.

Cell Culture

The cell lines used in this chapter were previously described in Chapter 3. Refer to Table 3.1 for cell descriptions. HAECs, HUVECs, and BEAS-2B cells were grown in 6-well plates (BD Falcon; Fisher Scientific, USA). HAECs and BEAS-2B cells were treated at 70% confluence with 10-nm $Si0_2$ (Nanostructured & Amorphous Materials, Inc., Houston, TX). HUVECs were treated at 70% confluence 70-nm (Z-PS-SIL-004-0,07, Postnova Analytics Landsberg, Germany) $Si0_2$ as part of a different experimental matrix but the data are

presented in this Chapter to confirm HAEC data in a second vascular cell line. Camptothecin (Sigma Aldrich, St Louis, MO) was used as a positive control for the induction of apoptosis. To investigate the role of ROS in cellular apoptosis, cells were pretreated with 5 mM *N*-acetyl-L-cysteine (NAC) (Sigma Aldrich, St Louis, MO) before treatment with particles.

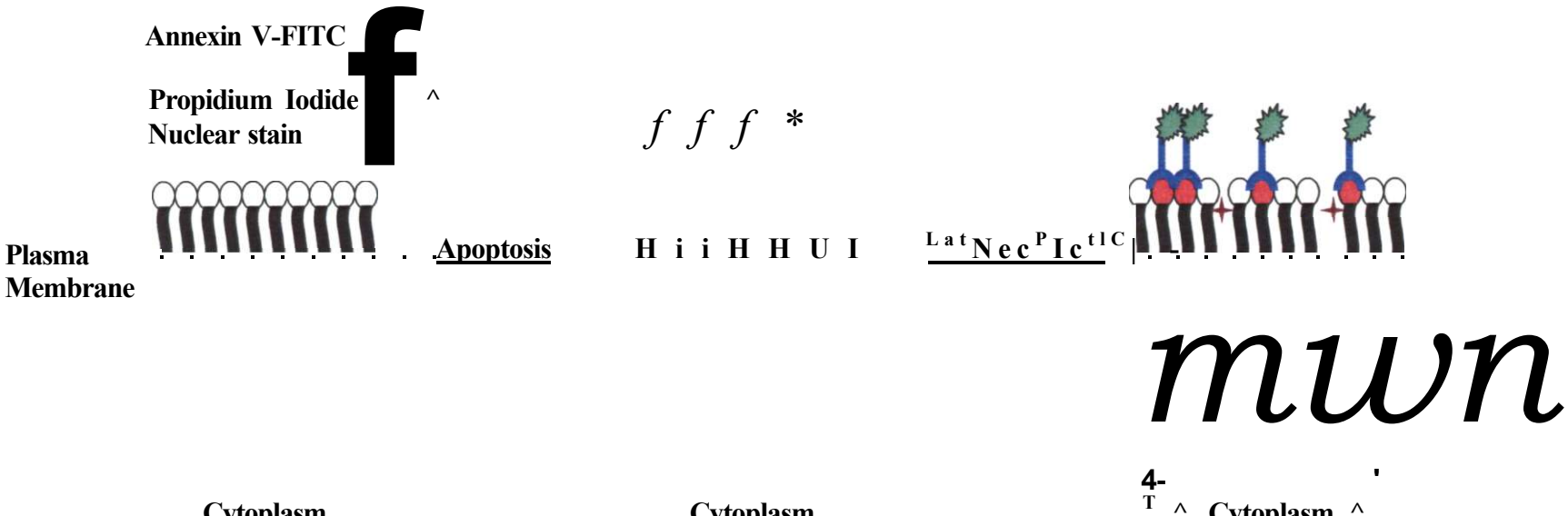

Figure 4.1 Apoptosis - Annexin V-FITC diagram

Apoptosis Assay

Apoptosis was measured using Vybrant® Apoptosis Assay Kit #3 (Molecular Probes, Eugene, OR). After a 24 hour treatment, culture media was removed, cells were trypsin-dissociated and added back to the previously removed culture medium. The cells were centrifuged at 200 x g for 5 minutes. The pellet was washed two times with ice cold PBS. The final pellet was resuspended in AV-binding buffer provided in the kit. Samples were incubated for 15 minutes with propidium iodide (PI) and FITC-conjugated AV before analysis on a Cell Lab Quantum Flow Cytometer (Beckman Coulter, Fullerton, CA).

Results

Apoptosis in Multiple Cell Lines

The flow cytometry data obtained from a control sample is represented in Figure 4.2. The two dyes used in this assay are PI and AV. PI is a cell impermeable nuclear dye used to determine cell viability by assessing membrane permeability. AV belongs to the family of proteins known as the annexins. Annexins are anticoagulants but have been found to preferentially bind to negatively charged phospholipids like PS in the presence of Ca^{2+}. Binding of AV to PS permits the detection and quantification of apoptosis. The results are presented as a cell plot with four quadrants. As indicated in Figure 4.2, the separate quadrants are as follows: PI positive AV negative cells (Ql), PI and AV positive cells (Q2), AV positive PI negative cells (Q4) and PI and AV negative cells (Q3). When cells are stained positive for both FITC and PI, this is indicative of late apoptotic or necrotic cells since PS is externalized and PI is able to enter the cells. Since the cell population in this quadrant is not fully characterized as either late apoptotic or necrotic it is not useful for the

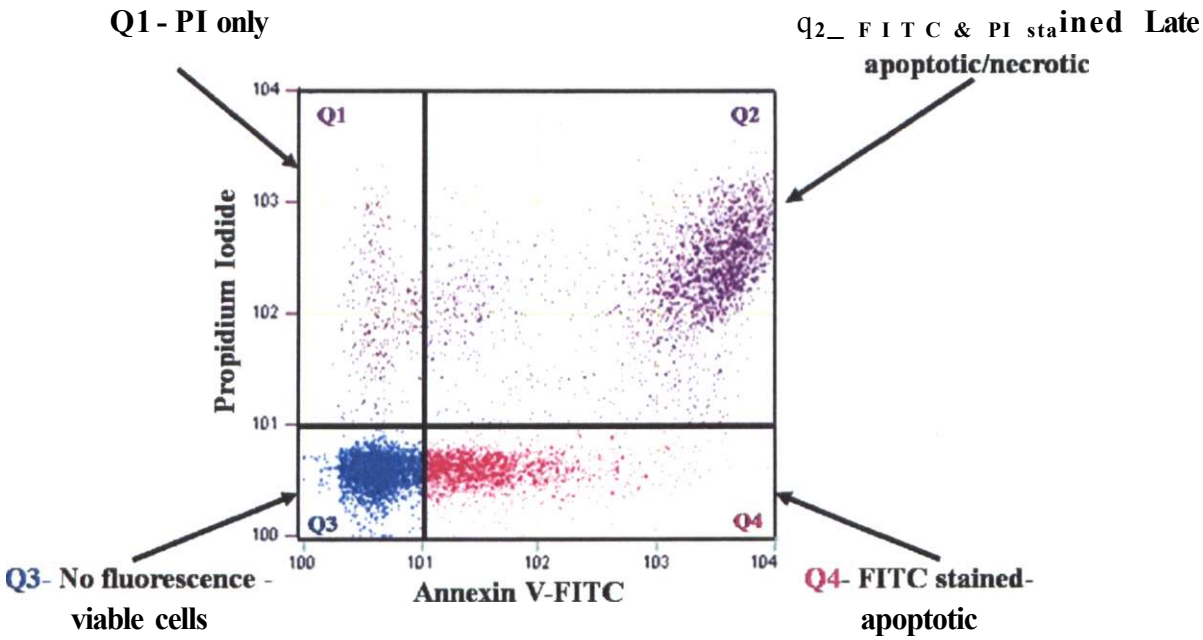

Figure 4.2 Representative cell gating by flow cytometry for the untreated control. Cells stained with the different dyes are represented in each quadrant as labeled. Q4 represents the percentage of apoptotic cells and will be used for the quantification of apoptosis.

measurement of apoptosis. The quadrant that will be used for the determination of apoptosis is Q4. The only signal measured in this quadrant is from AV-FITC binding, indicating that these cells are undergoing apoptosis, as measured by the externalization of phosphatidylserine.

Figure 4.3 graphically represents the apoptosis assay data from HAEC treated with increasing doses of silica for 24 hours. Camptothecin, an anti-cancer drug, was used as a positive control to induce DNA damage. Camptothecin acts by stabilizing topoisomerase I, preventing re-ligation of DNA, resulting in apoptosis. For almost all of the treatments, the percentage of cells in Q1 is negligible and the percent of cells in late apoptosis/necrosis is relatively low with the exception of cells treated with 31.6 pg/cm SiC>2. In Chapter 3, this dose was shown to be significantly cytotoxic and these results confirm this previous observation. Untreated cells are 60% viable with roughly 25% of cells staining positive for AV. A basal level of AV staining is typical for most cell lines since there is a certain amount of PS always present on the external surface of the cell membrane. All other treatments show increases of FITC-stained cells over control with minor changes in FITC-PI staining. Figure 4.4 shows the percentage of cells from Q4 representing apoptosis. Our positive control has increased significantly over untreated controls in both HAECs and HUVECs. Silica treatment also significantly increases the percentage of apoptotic cells, showing that our positive control and silica treatments induce apoptosis in vascular cells.

Data from previous chapters have shown a lack of pulmonary cell response to silica until the upper limits of doses tested. Figure 4.5 graphically represents the data from FITC-conjugated Annexin V stained BEAS-2B cells. Silica failed to induce significant apoptosis with concentrations up to 31.6 pg/cm^2. At 100 pg/cm^2, significant FITC-PI staining was

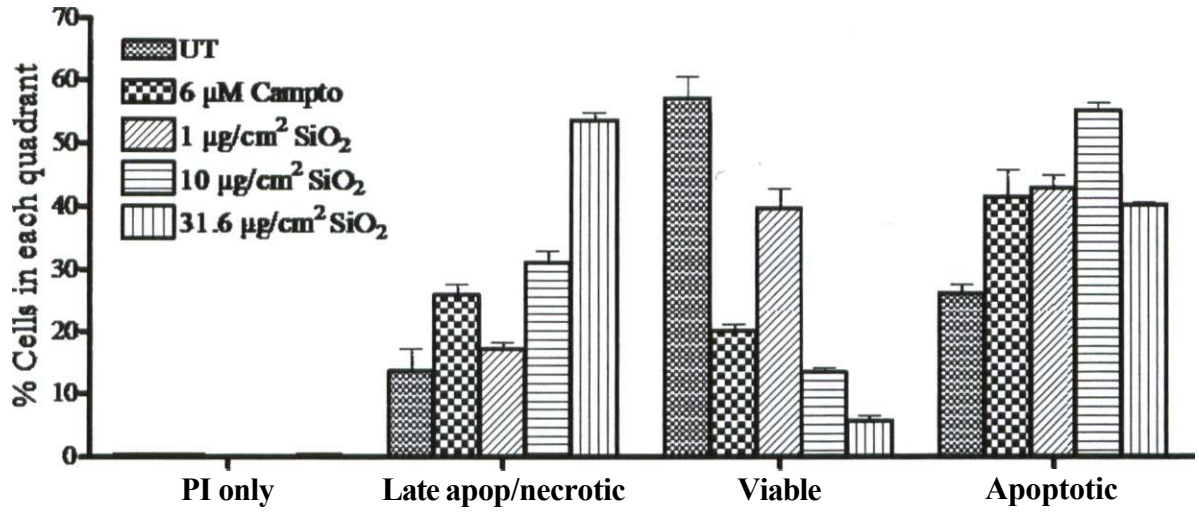

Figure 4.3 Percent HAECs in each quadrant after treatment with 10 nm SiO2. HAECs were treated for 24 hours with silica nanoparticles, camptothecin or were untreated (UT). Data are representative of all of the data obtained from the Annexin V flow cytometer assay. Data are represented as percent of cells in each quadrant. Each bar represents n=3.

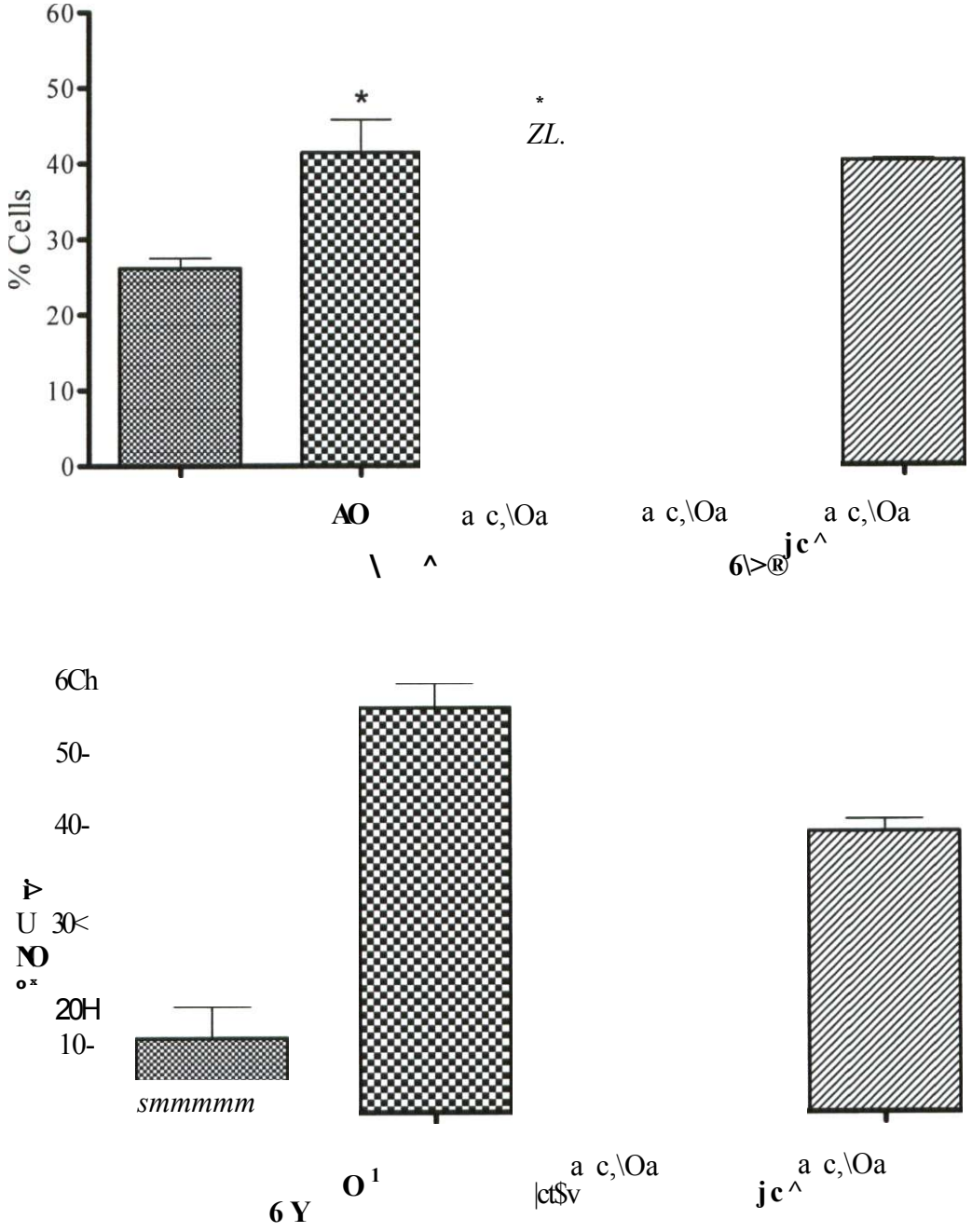

Figure 4.4 Apoptosis in vascular cells treated with $Si0_2$. A. HAECs treated with Camptothecin (positive control) and increasing doses of 10 nm $Si0_2$ for 24 hours or were untreated (UT). B. HUVECs treated with Camptothecin (positive control) and 70 nm $Si0_2$ for 24 hours. Data are represented as percent of cells in the apoptotic quadrant. Each bar represents n=3. Statistically significant changes (student's /-test, $p<0.05$) are identified with an asterisk (*).

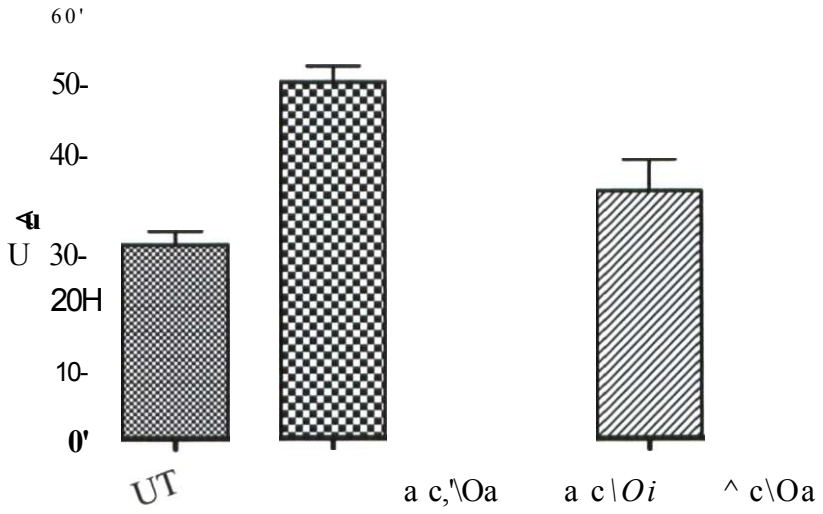

Figure 4.5 Apoptosis in BEAS-2B cells. Cells were untreated (UT) or were treated with increasing doses of 10 nm SiO2, harvested at 24 hours and apoptosis measured. Camptothecin was used as a positive control. Data are represented as percent of cells in the apoptotic quadrant (Q4). Statistically significant changes (student's /-test, $p<0.05$) are identified with an asterisk (*).

observed (data not shown), which meant that this high concentration killed most of the lung cells. Therefore, SiC>2 did not appear to cause apoptosis, but was cytotoxic at the highest concentration.

The Role of ROS in Apoptosis

To investigate the role of ROS in apoptosis, cells were pretreated with NAC, a metabolite of the amino acid Cysteine. NAC acts directly as an antioxidant, reducing free radicals or is converted to L-cysteine, a precursor to glutathione, a potent antioxidant. The results from pretreatment of NAC before a co-treatment with Si02 is shown in Figure 4.6. Experiments were performed to determine the most effective, nontoxic and nonapoptotic concentration of NAC which was 5 mM (data not shown). Pretreatment with NAC ameliorated almost all of the Si02-induced apoptosis.

Discussion

The studies in this chapter investigated the mechanism of nanosilica-induced vascular cell damage. Amorphous nanosilica is the particle used through this dissertation because it was generally believed to be benign, and therefore could potentially be useful in many medical applications. This assumption appears to be valid for the BEAS-2B lung cells, because silica did not significantly induce cell death via any mechanism including apoptosis as measured by the Annexin V or PI staining, until a concentration of 100 pg/cm was applied. At these doses the cells stained positive for both annexin and PI, indicating that the cells died via necrosis or were in the late stages of apoptosis. However, since lower doses did not show signs of apoptosis, cell death was most likely through necrosis.

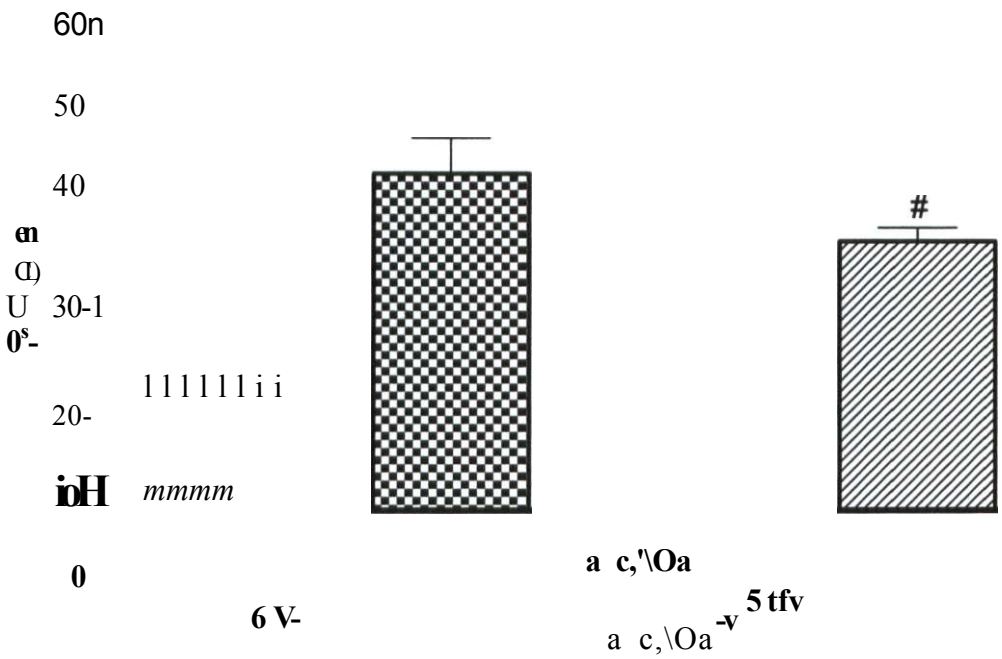

Figure 4.6 Evaluating the role of ROS in HAEC apoptosis. Cells were untreated (UT), treated with 10 nm Si02, or were treated with NAC then co-treated with 10 nm Si02 for 24 hours. Camptothecin was used as a positive control. Data are represented as percent of cells in the apoptotic quadrant. Each bar represents n=4 (n=2 from 2 independent passages). Results statistically significant from control are identified with an asterisk (*) or from Si02-treated cells are identified with a pound sign (#) (student's Mest, $p<0.05$).

Many studies involving silica induced apoptosis in pulmonary cells have focused on crystalline silica. These studies have shown a substantial induction of apoptosis due to micron-sized crystalline silica treatment [115-118]. The study of micron-sized crystalline silica is important to address occupational exposures and the etiology of the well characterized syndrome known as silicosis. Since silicosis is a severe condition, evaluations of the mechanisms of cell damage may help prevent or treat the syndrome. One proposed mechanism in which particles causes apoptosis is through the production of reactive oxygen species. Hu *et al.* showed that silica-induced apoptosis in alveolar macrophages is inhibited by the pretreatment of cells with the antioxidants, NAC and rhodamine 6G [120]. This work is similar to ours only using a crystalline form of $Si0_2$ in alveolar macrophages. In addition to inhibiting apoptosis, they also showed that NAC inhibited silica-induced production of IL-1β and tumor necrosis factor alpha [120].

While research into the cause of silicosis is not directly related to the research presented here, the methodologies used to determine the cause of apoptosis may translate to other particles and cell types. Current research by Santarelli *et al.* showed that HAECs treated with a-Quartz (Min-U-Sil 5) for 18 hours were positive for FITC-conjugated annexin V and confirmed their results using the Tunnel assay, another measurement of apoptosis [119]. Their study also showed ROS generation induced by crystalline silica was inhibited by treatment with 1,3-dimethyl-2-thiourea (DMTU), a hydroxyl radical scavenger [119]. Although the studies presented in this chapter utilized amorphous instead of crystalline silica, significant induction of apoptosis was seen in both HAECs and HUVECs. In fact, doses of 1 pg/cm^2 produced significant apoptosis in HAECs equal to that of the positive control.

ROS is a common endpoint measured after treatment with particles because the particle surface itself can facilitate the production of ROS, and particles can interact with cells to induce intra and extracellular ROS [82-85]. These observations do not hold true for every particle. In fact, a recent study has shown that yttrium oxide and cerium oxide actually act as antioxidants in neurons [121].

Our studies showed pretreatment with NAC prior to exposure substantially reduced the percentage of apoptotic cells staining positive for apoptosis. This suggests that ROS is involved in apoptosis induced by silica nanoparticles. However, since the percentage of cells staining positive for apoptosis did not completely return to control levels, other mechanisms may contribute to the induction of apoptosis. A future direction for this research would be to determine the site of ROS generation, whether it be mitochondrial, lysosomal, or extracellular. Assays assessing the mitochondrial depolarization, a site of ROS generation and signaling for apoptosis, as well as caspase activation assays would give further insight into the mechanism behind silica-induced ROS generation and apoptosis. The induction of antioxidant genes such as NQO1 (NAD(P) H: quinone oxidoreductase), superoxide dismutase (SOD), heme oxygenase 1, and glutathione S-transferase (GST) can be used as biomarkers for the presence of ROS. Induction of these genes would indicate a sustained substantial presence of reactive species which these genes might aid in detoxifying. Analysis of NQO1 gene induction was performed. However, preliminary results were inconclusive (data not shown). Inhibition of ROS may also decrease the production of proinflammatory cytokines as was seen by Hu *et al.* [120]. Additionally, other mechanisms of apoptosis should be assessed such as particle induced DNA damage leading to apoptosis as well as

testing more vascular cell lines to determine if the results are specific to HUVEC and HAEC cells.

The data presented in this chapter show that treatment with amorphous nanosilica induces apoptosis in vascular cells. By showing that inhibition of ROS formation can ameliorate apoptosis, we have contributed to understanding how nanoparticles cause vascular cell death. With these exciting results, additional research can be conducted to further understand the toxicity of nanoparticles and aid in producing a "safer" formulation that can be used for biomedical research.

CHAPTER 5

CONCLUSIONS

Overview

Respiratory and cardiovascular morbidity and mortality are attributed to exposure to particles found in environmental air pollution. With the advances in technology and the attractiveness of nanoparticle chemistry, scientists have begun to introduce nanoparticles into various scientific fields. Already there are over 600 consumer products incorporating nanotechnology [11]. While inhaled micron-sized particles have long been correlated with lung disease and cardiovascular effects, the specific effects of nanoparticles are largely understudied until recently. Nanoparticles may have vastly different properties from that of closely related larger, micron-sized particles. Emerging human toxicological profiles suggest both the potential for unique therapeutic applications, as well as unusual adverse effects.

The newest and most interesting uses for nanoparticles are as medical diagnostic tools and carriers for drug delivery. Metal oxide particles were used extensively in the studies presented in this document because they are not only present in air pollution, but they are also used 1) as components of electronics; 2) as vehicles for drug [16-18] and gene [19, 20] delivery in the biomedical field; 3) as imaging probes [21]; and 4) as disease diagnostic tools.

Many reports on the adverse effects of nanoparticles have focused on inhalation and associated lung diseases. However, these processes have yet to be fully characterized. Emerging evidence has shown that particles can translocate from the lung to the systemic circulation [22, 24, 32-35]. Thus, it is vital to determine tissue distribution and toxicities of these particles. Currently there is no clear method to determine organ-specific exposures to adsorbed, inhaled, ingested or injected nanoparticles without specific labels to detect their presence. We address this problem by modifying the methodology of field-flow fractionation, to provide a useful new method to simultaneously quantitate nanoparticle amounts and determine size distribution.

General exposure to particulates through inhalation, injection and ingestion provide routes for contact of nanoparticles with pulmonary epithelial, vascular endothelial and colorectal epithelial cells. Current research from various groups has attempted to access particle toxicities in these organ systems. However, comprehensive direct comparisons have not been made because different particulates and different biological materials and techniques have been utilized to measure common endpoints. In Chapters 3 and 4, concurrent cell culture experiments are performed to directly compare cell types treated with the same particles, with the goals to determine the mechanism by which particles induce cellular damage and to rank the relative susceptibilities of these three organs.

Chapter 2

In Chapter 2 the capability to detect nanoparticles and to simultaneously distinguish particle size distribution for unlabeled SiO_2 in a sample of mammalian lung tissue was demonstrated. Pre-existing techniques were used in combination, permitting

separation of particulates from biological matrix. Isolating silicon dioxide from liver and the more structurally complicated lung was a very important step in the overall analysis of particle concentrations in tissue. The current methodologies for the identification and quantification of particles in tissue, fluorescence microscopy and TEM, were compared to our sample analysis with the SdFFF instrument, demonstrating the usefulness of microscopy to show particle interactions with cells, and to show the effectiveness of our enzyme digestion and particle separation techniques. SdFFF of control particles suspended in surfactant was used to generate a standard curve. The limit of detection was 7×10^{10} particles per injected sample using a light scattering detector. In the future, coupling the SdFFF instrument to ICP-MS would greatly enhance the sensitivity of detection, and could be used to determine the composition of each peak from a tissue sample.

Our methodology is able to detect unlabeled Si02 nanoparticles isolated from rat lung and liver tissue, but more importantly, is able separate a mixture of silica nanoparticles with nominal diameters of 70 and 250 nm, illustrating the exciting capability of the SdFFF methodology to detect nano- and submicron-sized particles from the same tissue in a single run with high resolution. The combination of enzyme digestion of tissue with particle sizing by SdFFF is a novel approach that will greatly facilitate measurements of natural and anthropogenic nanoparticles in laboratory toxicology studies, ecological systems, and human populations. This work introduces a new method to characterize the size distribution of unlabeled inorganic particles in tissue, which will be beneficial for studies focused on the cardiovascular effects of

environmental and occupational exposures to an important class of engineered nanomaterials.

Chapter 3

In Chapter 3, a complex matrix including multiple cell lines was used to assess the toxicity of the metal oxide nanoparticles silicon dioxide, titanium dioxide, iron oxide, zinc oxide and cerium oxide. Previous studies have shown that metal oxide particles are not highly toxic or proinflammatory in the pulmonary cell line, BEAS-2B [102]. An assay that measures mitochondrial function to assess cellular viability showed a dose response to the metal oxide nanoparticles with the vascular endothelial cells, HAEC and HUVECs. The pulmonary (NHBE and BEAS-2B) and colorectal (CaCo-2 and RKO) epithelial cell lines were affected by only the highest concentrations tested and loss of viability was rarely statistically significant. The LD_{50} of all of the particles in all of the cells showed that vascular cells were considerably more sensitive to metal oxide particle exposures with both micron-sized and nano-sized particles, in respect to cell death. Our results are consistent with other reports on effects in the respiratory tract. The enhanced sensitivity of vascular cells may be due to the difference in cellular functions compared to that of pulmonary and colon cell lines. Vascular cells are not typically exposed to irritants and chemicals as frequently as the cells of the lung and colon which have direct contact with inhaled or ingested items.

Cytokine production, a marker for cellular risk, was assessed, providing additional evidence that vascular cells are more sensitive to metal oxide nanoparticles than pulmonary or colorectal cells. In terms of the most likely applications of nanoparticle uses, enhanced sensitivity of the vascular endothelium to particulates could

be particularly deleterious when metal oxide nanoparticles are used in the medical field, because these particles are most likely going to be injected and would encounter vascular cells frequently and at high concentrations. Formulations of nanoparticles used in the biomedical field are being produced to enhance their safety. However, since incidental and environmental metal oxide nanoparticles can be present in air pollution as a result of windblown dust, regulation of their size, shape and chemistry is difficult. The vascular effects that we have shown may explain the increased cardiovascular morbidity and mortality observed after exposure to high concentrations of air pollution.

Chapter 4

In Chapter 4 the complex matrix of experiments was simplified to focus on only one metal oxide nanoparticle with vascular and pulmonary cells. The purpose of simplifying the experimental matrix was to investigate a mechanism by which a specific oxide nanoparticle, such as nanosilica, alters vascular cell function. BEAS-2B cells showed only minor responses to silica in Chapter 3, which was consistent with the results in Chapter 4. Apoptosis did not become significant in BEAS-2B cells (measured by Annexin V or PI staining) until a concentration of 100 pg/cm^2 was used. Other forms of silica have shown a substantial induction of apoptosis in pulmonary cells [115-118], However, those silica forms were not nano-sized and would not be used in most medical applications.

Vascular cells, which responded significantly to silica in Chapter 3, showed significant induction of apoptosis at low, near physiologically relevant concentrations. In addition, apoptosis, measured by the externalization of PS, was prevented when vascular cells were pretreated with the antioxidant, NAC. Therefore, one mechanism for the

induction of cellular death by nano-sized silica probably occurs through the formation of ROS.

Future Directions

While this study has provided remarkable progress in the identification and understanding of nanoparticles, further research is still required. The SdFFF data presented here showed that our tissue digestion followed by SdFFF can be used to detect particles isolated from tissues. However to fully utilize this technique, additional characterization is required. The limit of detection can be improved by using ICP-MS, permitting the determination of particle concentration and particle composition. Additionally, understanding and preventing particle loss during tissue processing will be necessary to make this assay truly quantitative. The major goal is to expose an animal to particles and be able to isolate each tissue, precisely measuring deposited particle concentrations.

Knowing the concentration of particulates in tissue is important for extrapolating *in vivo* exposures to *in vitro* studies. Our results show that vascular cells respond to nanosilica by the production of proinflammatory cytokines and the induction of cellular apoptosis, which is preventable by pretreatment with an antioxidant. Future research should focus on the link between all of these effects (ROS, apoptosis and inflammation). Previous studies with micron-sized crystalline particles have begun to investigate the link between apoptosis and ROS [120]. Modeling our studies after their results may show similar patterns. Investigating the point in the signal transduction pathway that is activated and leads to apoptosis would permit us to understand the site of particle-induced alterations. One pathway to investigate is the activation of the TNF-a receptor.

As stated in Chapter 1, particles and ROS induce the production of TNF-a, which can bind to the TNF-a receptor on the surface of a cell, and activate the external apoptosis pathway.

Another future direction for this research would be to directly detect the presence of ROS. Our initial studies showed that antioxidants were able to ameliorate apoptosis. However, we did not directly measure ROS. Changes in the gene induction of GST, SOD, NQOl and many other antioxidant genes, using a reporter assay or quantitative real-time PCR could be used to identify the presence of ROS. Other techniques such as spin trapping will directly detect the presence of free radical components of ROS. If we confirm ROS production, determination of the site of ROS generation, whether it is mitochondrial, lysosomal, or extracellular would be beneficial and provide further mechanistic evidence that could link particle-induced ROS processes and apoptosis. Since our research has shown an increase in proinflammatory cytokine production, determining the alteration of these cytokines in the presence of an antioxidant may yield important information about the toxicity of nanoparticles.

Final Statement

The work presented in this document contributed to the overall understanding of nanoparticles toxicology. A new method to identify unlabeled inorganic nanoparticles in tissue was demonstrated and evidence was provided showing that vascular endothelial cells have enhanced sensitivity to metal oxide nanoparticles that may be mediated by the production of ROS, leading to cellular apoptosis. Based on our results, the use of nano-sized Si02 in the biomedical field may have serious consequences. Antioxidants are used in the treatment of many diseases, and have been shown to inhibit particle-induced

apoptosis in our studies. Therefore, it is possible that antioxidants may be used as potential therapies for persons exposed to high levels of metal oxide nanoparticles. This body of work has provided exciting new data that permits the progression and understanding of nanoparticle toxicology. With continued efforts, we may one day be able to fully understand nanoparticles and their cellular effects, and make them safe for all of the population.

REFERENCES

1. 2456-06 AE: **Terminology for nanotechnology.** *ASTM International* 2006.

2. Kulmala M, Vehkamaki H, Petaja T, Dal Maso M, Lauri A, Kerminen VM, Birmili W, McMurry PH: **Formation and growth rates of ultrafine atmospheric particles: a review of observations.** *Journal of Aerosol Science* 2004, **35**:143-176.

3. Oberdorster G, Oberdorster E, Oberdorster J: **Nanotoxicology: An emerging discipline evolving from studies of ultrafine particles.** *EHP* 2005, **113**:823-839.

4. Nemery B, Hoet PHM, Nemmar A: **The Meuse Valley fog of 1930: an air pollution disaster.** *The Lancet* 2001, **357**:704-708.

5. Logan WPD: **Mortality in the London fog incident, 1952.** *The Lancet* 1953, **261**:336-338.

6. Dominici F, McDermott A, Daniels M, Zeger S, Samet J: **Mortality among residents of 90 cities.** In *Special Report: Revised Analysis fo Time-Series Studies of Air Pollution and Health,* pp. 9-24. Boston: Health Effects Institute; 2003:9-24.

7. **Peak air quality statistics for the six principal pollutants by metropolitan statistical area, 2003 (Table)** [http://www.epa.gov/airtrends/pdfs/msafactbook-04.pdf]

8. Pope III CA: **Epidemiology of fine particulate air pollution and human health: biologic mechanisms and who's at risk?** *EHP* 2000, **108**:713-723.

9. Allen D, Fraser M: **An overview of the gulf coast aerosol research and characterization study: the Houston fine particulate matter supersite.** *J Air Waste Manag Assoc* 2006, **56**:456-466.

10. Phares DJ, Rhoads KP, Johnston MV, Wexler AS: **Size-resolved ultrafine particle compostion analysis part 2: Houston.** *Journal of Geophysical Research, [Atmospheres]* 2003, **108.**

11. Felcher ME: **Project on emerging nanotechnologies.** *The consumer product safety commission and nanotechnology* **2008, 14.**

12. The National Science and Technology Council, Committee on Technology, Subcommittee on Nanoscale Science E, and Technology,, Group NEaHIW: **The National Nanotechnology Initiative: Strategy for nanotechnology-related environmental, health, and safety research.** Washington, D.C.; 2008.

13. Rodriguez JA, Fernandez-Garcia M (Eds.): **Synthesis, properties, and applications of oxide nanopaterials.** Hoboken, New Jersey: John Wiley & Sons, Inc.,; 2007.

14. Klabunde KJ, Stark J, Koper O, Mohs C, Park DG, Decker S, Jiang Y, Lagadic I, Zhang D: **Nanocrystals as stoichiometric reagents with unique surface chemistry.** *The Journal of Physical Chemistry* 1996, **100**:12142-12153.

15. Schwarz JA, Contescu CI, Putyera K (Eds.): **Dekker Encyclopedia of Nanoscience and Nanotechnology:** CRC Press; 2004.

16. Heikkila T, Salonen J, Tuura J, Hamdy MS, Mul G, Kumar N, Salmi T, Murzin DY, Laitinen L, Kaukonen AM: **Mesoporous silica material TUD-1 as a drug delivery system.** *International Journal of Pharmaceutics* 2007, **331**:133-138.

17. Kortesuo **P,** Ahola **M,** Karlsson S, Kangasniemi **I,** Yli-Urpo A, Kiesvaara **J: Silica xerogel as an implantable carrier for controlled drug delivery—evaluation of drug distribution and tissue effects after implantation.** *Biomaterials* 2000, **21**:193-198.

18. Xue J, Tan C, Lukito D: **Biodegradable polymer-silica xerogel composite microspheres for controlled release of gentamicin.** *J Biomed Mater Res B Appl Biomater* 2006, **78**:417-422.

19. Bharali DJ, Klejbor I, Stachowiak EK, Dutta P, Roy I, Kaur N, Bergey E, Prasad PN, Stachowiak MK: **Organically modified silica nanoparticles:** A **nonviral vector for *in vivo* gene delivery and expression in the brain.** *PNAS* 2005, **102.**

20. Hoet **P,** Bruske-Hohlfeld **I,** Salata O: **Nanoparticles - known and unknown health risks.** *Journal of Nanobiotechnology* 2004, **2**:12.

21. Bakalova R. Zhelev Z, Aoki I, Ohba H, Imai Y, Kanno I: **Silica-shelled single quantum dot micelles as imaging probes with dual or multimodality.** vol. 78. pp. 5925-5932;2006:5925-5932.

22. Geiser M, Rothen-Rutishauser B, Kapp N, Schiirch S, Kreyling W, Schulz H, Semmler M, Im Hof V, Heyder **J,** Gehr **P: Ultrafine particles cross cellular membranes by nonphagocytic mechanisms in lungs and in cultured cells.** *Environmental Health Perspectives* 2005, **113**:1555-1560.

23. Ferin J, Oberdorster G, Penney DP, Soderholm SC, Gelein R, Piper HC: **Increased pulmonary toxicity of ultrafine particles? I. Particle clearance, translocation, morphology.** *Journal of Aerosol Science* 1990, **21**:381-384.

24. Kreyling WG, Semmler M, Erbe F, Mayer P, Takenaka S, Schultz H, Oberdorster G, Ziesenis A: **Translocation of ultrafine insoluble iridium particles from lung epithelium to extrapulmonary organs is size dependent but very low.** *Journal of Toxicology and Environmental Health Part A* 2002, 65:1513-1530.

25. Brook RD, Franklin B, Cascio W, Hong Y, Howard G, Lipsett M, Luepker R. Mittleman M, Samet J, Smith SC, Jr., Tager **I: Air pollution and cardiovascular disease: a statement for healthcare professionals from the expert panel on population and prevention science of the American Heart Association.** *Circulation* 2004, **109**:2655-2671.

26. Martin F, Melnik K, West T, Shapiro J, Cohen M, Boiarski A, Ferrari M: **Acute toxicity of intravenously administered micorfabricated silicon dioxide drug delivery particles in mice: preliminary findings.** *Drugs R D* 2005, 6:71-81.

27. Nel A, Xia T, Madler L, Li N: **Toxic potential of materials at the nanolevel.** *Science* 2006,311:622-627.

28. Kim JS, Yoon T-J, Yu KN, Kim BG, Park SJ, Kim HW, Lee KH, Park SB, Lee J-K, Cho MH. **Toxicity and tissue distribution of magnetic nanoparticles in mice.** vol. 89. pp. 338-347; 2006:338-347.

29. Chen M, von Mikecz A: **Formation of nucleoplastic protein aggregrates impairs nuclear function in response to $Si0_2$ nanoparticles.** *Experimental Cell Research* 2005, **305**:51-62.

30. Gamer AO. Leibold E, van Ravenzwaay B: **The in vitro absorption of microfine zinc oxide and titanium dioxide through porcine skin.** *Toxicology in Vitro* 2006, **20**:301-307.

31. Lomer MCE, Thompson RPH, Commisso J, Keen CL, Powell JJ: **Determination of titanium dioxide in foods using inductively coupled plasma optical emission spectrometry.** *The Analyst* 2000, **125**:2339-2343.

32. Nemmar A, Hoet PHM, Vanquickenborne B, Dinsdale D, Thomeer M, Hoylaerts MF, Vanbilloen H, Mortelmans L, Nemery B: **Passage of inhaled particles into the blood circulation in humans.** *Circulation* 2002, **105**:411-414.

33. Nemmar A, Vanbilloen H, Hoylaerts MF, Hoet PHM, Verbruggen A, Nemery B: **Passage of intratracheal^ instilled ultrafine particles from the lung into the systemic circulation in hamster.** *Am J Respir Crit Care Med* 2001, **164**:1665-1668.

34. Oberdorster G, Sharp Z, Atudorei V, Elder A, Gelein R, Lunts A, Kreyling W, Cox C: **Extrapulmonary translocation of ultrafine carbon particles following whole-body inhalation exposure of rats.** *Journal of Toxicology and Environmental Health Part A* 2002, 65:1531-1543.

35. Takenaka S, Karg E. Roth C, Schulz H, Ziesenis A, Heinzmann U, Schramel P, Heyder J: **Pulmonary and systemic distribution of inhaled ultrafine silver particles in rats.** *Environ Health Perspect* 2001, **109**:547-551.

36. Shimada A, Kawamura N, Okajima M, Kaewamatawong T, Inoue H, Morita T: **Translocation pathway of the intratracheal^ instilled ultrafine particles from the lung into the blood circulation in the mouse.** *Toxicol Pathol* 2006, **34**:949-957.

37. Boxall A, Tiede K, Chaudhry Q: **Engineered nanoparticles in soils and water: how do they behave and could they pose a risk to human health.** *Nanomedicine* 2007, **2**:919-927.

38. Sadauskas E, Wallin H, Stoltenberg M, Vogel U, Doering P, Larsen A, Danscher G: **Kupffer cells are central in the removal of nanoparticles from the organism.** *Part Fibre Toxicol* 2007, **4**:10.

39. Ryman-Rasmussen JP. Riviere JE, Monteiro-Riviere NA: **Penetration of intact skin by quantum dots with diverse physicochemical properties.** *Toxicological Sciences* 2006, **91**:159-165.

40. Elder A, Gelein R, Silva V, Feikert T, Opanashuk L, Carter J, Potter R, Maynard A, Ito Y, Finkelstein J, Oberdorster G: **Translocation of inhaled ultrafine manganese oxide particles to the central nervous system.** *Environmental Health Perspectives* 2006, 114:1172-1178.

41. Giddings JC: *Unified Separation Science.* New York: Wiley-Interscience; 1991.

42. Myers MN: **Overview of field-flow fractionation.** *Journal of Microcolumn Separations* 1997, 9:151-162.

43. Caldwell KD, Compton BJ, Giddings JC, Olson RJ: **Sedimentation field-flow fractionation: a method for studying particulates in cataractous lens.** *Investigative Ophthalmology & Visual Science* 1984, **25**:153-159.

44. Baalousha M, Lead JR: **Characterization of natural aquatic colloids (< 5 nm) by flow-field flow fractionation and atomic force microscopy.** *Environ Sci Technol* 2007, **41**:1111-1117.

45. Assemi S, Newcombe G, Hepplewhite C, Beckett R: **Characterization of natural organic matter fractions separated by ultrafiltration using flow field-flow fractionation.** *Water Research* 2004, **38**:1467-1476.

46. Lead JR, Wilkinson KJ, Balnois E, Cutak BJ, Larive CK, Assemi S, Beckett R: **Diffusion coefficients and polydispersities of the suwannee river fulvic acid: comparison of fluorescence correlation spectroscopy, pulsed-field gradient nuclear magnetic resonance, and flow field-flow fractionation.** *Environ Sci Technol* 2000, **34**:3508-3513.

47. Chun J, Fagan J, Hobbie E, Bauer B: **Size separation of single-wall carbon nanotubes by flow-field flow fractionation.** *Analytical Chemistry* 2008, **80**:2514-2513.

48. Schimph ME, Caldwell KD, Giddings JC (Eds.): **Field-Flow Fractionation Handbook** New York: John Wiley & Sons, Inc.; 2000.

49. Takjiki S, Assemi S, Deering CE, Veranth JM, Miller JD: **Detection, separation, and quantification of unlabeled silica nanoparticles in biological media using sedimentation field-flow fraction.** *J Nanoparticle Research accepted for publication* 2008.

50. Giddings JC, Ratanathanawongs SK, Moon MH: **Field-flow fractionation: a versatile technology for particle characterization in the size range 10^3 to 10^2.** *Kona: Powder and Particle* 1991, 9:200-217.

51. Veranth J: **In vitro models for nanoparticle toxicology.** In; 2009

52. **International Commission on Radiological Protection Task Force on Lung Dynamics.** *Health Phys* 1966,**12**:173-207.

53. Guyton AC, Hall JE: *Textbook of Medical Physiology*. Philadelphia, PA: Saunders; 1996.

54. Phalen RF, Oldham MJ, Nel AE: **Tracheobronchial Particle Dose Considerations for In Vitro Toxicology Studies.** *Toxicol Sci* 2006, **92:**126-132.

55. Teeguarden JG, Hinderliter PM, Orr G, Thrall BD, Pounds JG: **Particokinetics *in vitro*: Dosimetry considerations for *in vitro* nanoparticle toxicity assessments.** *Toxicological Sciences* 2007, **95**:300-312.

56. Lison D, Thomassen LCJ, Rabolli V, Gonzalez L, Napierska D, Seo JW, Kirsch-Volders M, Hoet P, Kirschhock CEA, Martens JA: **Nominal and effective dosimetry of silica nanoparticles in cytotoxicity assays.** *Toxicol Sci* 2008, **104**:155-162.

57. Driscoll KE: **Cytokines and regulation of pulmonary infalmation** In *Toxicology of the Lung.* Edited by Gardner D, Crapo J, McClellan R. Ann Arbor: Taylor & Francis; 1999: 149-172

58. Ghio AJ, Kim C, Devlin RB: **Concentrated ambient air particles induce mild pulmonary inflammation in healthy human volunteers.** *Am J Respir Crit Care Med* 2000, **162**:981-988.

59. Ghio AJ, Devlin RB: **Inflammatory lung injury after bronchial instillation of air pollution particles.** *Am J Respir Crit Care Med* 2001, **164**:704-708.

60. Quay JL, Reed W, Samet J, Devlin RB: **Air pollution particles induce IL-6 gene expression in human airway epithelial cells via NF-kappa B activation.** *Am J Respir Cell Mol Biol* 1998, **19**:98-106.

61. Kennedy T, Ghio AJ, Reed W, Samet J, Zagorski J, Quay J, Carter J, Dailey L, Hoidal JR, Devlin RB: **Copper-dependent Inflammation and Nuclear Factor-kappa B Activation by Particulate Air Pollution.** *Am J Respir Cell Mol Biol* 1998,**19**:366-378.

62. Fujii T, Hayashi S, Hogg JC, Vincent R, Van Eeden SF: **Particulate matter induces cytokine expression in human bronchial epithelial cells.** *Am J Respir Cell Mol Biol* 2001, **25**:265-271.

63. Jimenez LA, Drost EM, Gilmour PS, Rahman I, Antonicelli F, Ritchie H, MacNee W, Donaldson K: **PMlO-exposed macrophages stimulate a proinflammatory response in lung epithelial cells via TNF-alpha.** *Am J Physiol Lung Cell Mol Physiol* 2002, **282** :L237-248.

64. Goto Y, Ishii H, Hogg JC, Shih C-H, Yatera K, Vincent R, van Eeden SF: **Particulate matter air pollution stimulates monocyte release from the bone marrow.** *Am J Respir Crit Care Med* 2004, **170**:891-897.

65. Nemmar A, Hoylaerts MF, Hoet PHM, Dinsdale D, Smith T, Xu H, Vermylen J, Nemery B: **Ultrafine particles affect experimental thrombosis in an *in vivo* hamster model.** *Am J Respir Crit Care Med* 2002, **166**:998-1004.

66. Peters A, Frohlich M, Doring A, Immervoll T, Wichmann HE, Hutchinson WL, Pepys MB, Koenig W: **Particulate air pollution is associated with an acute phase response in men. Results from the MONICA-Augsburg Study.** *Eur Heart J* 2001. **22**:1198-1204.

67. Brook RD, Brook JR, Urch B, Vincent R, Rajagopalan S, Silverman F: **Inhalation of fine particulate air pollution and ozone causes acute arterial vasoconstriction in healthy adults.** *Circulation* 2002, **105**:1534-1536.

68. Faxon DP, Fuster V. Libby P, Beckman JA, Hiatt WR, Thompson RW, Topper JN, Annex BH, Rundback JH, Fabunmi RP. et al: **Atherosclerotic vascular disease conference: writing group III: pathophysiology.** *Circulation* 2004, **109**:2617-2625.

69. Corti R, Fuster V, Badimon J: **Pathogenetic concepts of acute coronary syndromes.** *J Am Coll Cardiol* 2003, **41**:S7-S14.

70. Pekkanen J, Peters A, Hoek G, Tiittanen P, Brunekreef B, de Hartog J, Heinrich **J,** Ibald-Mulli A, Kreyling WG, Lanki T, et al: **Particulate air pollution and risk of ST-segment depression during repeated submaximal exercise tests among subjects with coronary heart disease: The Exposure and Risk Assessment for Fine and Ultrafine Particles in Ambient Air (ULTRA) study.** *Circulation* 2002,**106**:933-938.

71. Peters A, Dockery DW, Muller JE, Mittleman MA: **Increased particulate air pollution and the triggering of myocardial infarction.** *Circulation* 2001, **103**:2810-2815.

72. Studzinski GP (Ed.). **Apoptosis - A Practical Approach.** New York: Oxford University Press; 1999.

73. Bouchier-Hayes L, Lartigue L, Newmeyer DD: **Mitochondria: pharmacological manipulation of cell death.** *J Clin Invest* 2005, **115**:2640-2647.

74. Kumar S (Ed.). **Apoptosis: mechanisms and role in disease:** Springer; 1998.

75. Balasubramanian K, Mirnikjoo B, Schroit AJ: **Regulated externalization of phosphatidylserine at the cell surface: Implications for apoptosis.** *J Biol Chem* 2007, **282**:18357-18364.

76. Surh Y-J, Packer L (Eds.): **Oxidative Stress Inflammation and Health:** CRC press; 2005.

77. Marcus DL, Thomas C, Rodriguez C, Simberkoff K, Tsai JS, Strafaci JA, Freedman ML: **Increased peroxidation and reduced antioxidant enzyme activity in Alzheimer's Disease.** *Experimental Neurology* 1998, **150**:40-44.

78. Harman D: **Free radical theory of aging: A hypothesis on pathogenesis of senile dementia of the Alzheimer's type.** *AGE* 1993, **16**:23-30.

79. Volicer M: **Free radicals in the development of Alzheimer's disease.** *Neurobiol Aging* 1990, **11**:567-571.

80. Sachidanandam K, Fagan S, Ergul A: **Oxidative stress and cardiovascular disease: antioxidants and unresolved issues.** *Cardiovasc Drug Rev* 2005, **23**:115-132.

81. Garewal HS (Ed.). **Antioxidants and disease prevention:** CRC Press; 1997.

82. Fubini B, Hubbard A: **Reactive oxygen species (ROS) and reactive nitrogen species (RNS) generation by silica in inflammation and fibrosis.** *Free Radical Biology and Medicine* 2003, **34**:1507-1516.

83. Kamp DW, Weitzman SA: **The molecular basis of asbestos induced lung injury.** *Thorax* 1999, **54**:638-652.

84. Shukla A, Gulumian M, Hei TK, Kamp D, Rahman Q, Mossman BT: **Multiple roles of oxidants in the pathogenesis of asbestos-induced diseases.** *Free Radical Biology and Medicine* 2003, **34:**1117-1129.

85. Donaldson K. Stone V, Seaton A, MacNee W: **Ambient patricle inhalation and the cardiovascular system: potential mechanisms.** *EHP* 2001, **109**:523-527.

86. Schoonen MAA, Cohn CA, Roemer E, Laffers R. Simon SR, O'Riordan T: **Mineral-induced formation of reactive oxygen species.** *Reviews in Mineralogy and Geochemistry* 2006, **64:**179-221.

87. Pierce G, Parchment R, Lewellyn A: **Hydorgen peroxide as a mediator of programmed cell death in blastocyst.** *Differentiation* 1991, **46**:181-186.

88. Simon H-U, Haj-Yehia A, Levi-Schaffer F: **Role of reactive oxygen species (ROS) in apoptosis induction.** *Apoptosis* **2000, 5:415-418.**

89. Basuroy S, Bhattacharya S, Tcheranova D, Qu Y, Regan RF, Leffler CW, Parfenova H: **HO-2 provides endogenous protection against oxidative stress and apoptosis caused by TNF-{alpha} in cerebral vascular endothelial cells.** *Am J Physiol Cell Physiol* 2006, **291** :C897-908.

90. Gloire G, Legrand-Poels S, Piette J: **NF-[kappa]B activation by reactive oxygen species: Fifteen years later.** *Biochemical Pharmacology* 2006, **72**:1493-1505.

91. Cheranov SY, Jaggar JH: **TNF-{alpha} dilates cerebral arteries via NAD(P)H oxidase-dependent Ca2+ spark activation.** *Am J Physiol Cell Physiol* 2006, **290**:C964-971.

92. Imoto K, Kukidome D. Nishikawa T, Matsuhisa T, Sonoda K, Fujisawa K, Yano M, Motoshima H, Taguchi T, Tsuruzoe K, et al: **Impact of mitochondrial reactive oxygen species and apoptosis signal-regulating kinase 1 on insulin signaling.** *Diabetes* 2006, 55:1197-1204.

93. Zamzami N, Marchetti P, Castedo M, Decaudin D, Macho A, Hirsch T, Susin SA, Petit PX, Mignotte B. Kroemer G: **Sequential reduction of mitochondrial transmembrane potential and generation of reactive oxygen species in early programmed cell death.** *J Exp Med* 1995, **182**:367-377.

94. Deering C, Tadjiki S, Assemi S, Miller J, Yost G, Veranth J: **A novel method to detect unlabeled inorganic nanoparticles and submicron particles in tissue by sedimentation field-flow fractionation.** *Particle and Fibre Toxicology* 2008, 5:18.

95. Blau **P,** Zollars **RL: Sedimentation field-flow fractionation of nonspherical particles.** *Journal of Colloid and Interface Science* 1996, **183**:476-483.

96. Grigg J, Kulkarni N, Pierse N, Rushton L, O'Callaghan C, Rutman A: **Black-Pigmented Material in Airway Macrophages from Healthy Children: Association with Lung Function and Modeled PM10.** In *Health Effects Institute Research Report*, vol. 134; 2008.

97. Saxena RK, Gilmour MI, Hays MD: **Isolation and quantitative estimation of diesel exhaust and carbon black particles ingested by lung epithelial cells and alveolar macrophages in vitro.** *BioTechniques* 2008, **44**:799-805.

98. Kim Ws, Kim SH, Lee DW, Lee S, Lim CS, Ryu JH: **Size Analysis of Automobile Soot Particles Using Field-Flow Fractionation.** *Environ Sci Techno/* 2001**,35**:1005-1012.

99. Park YH, Kim WS, Lee DW: **Size analysis of industrial carbon blacks by sedimentation and flow field-flow fractionation** *Analytical and Bioanalytical Chemistry* 2003, **375**:489-495.

100. Warheit DB, Webb TR, Colvin VL, Reed KL, Sayes CM: **Pulmonary bioassay studies with nanoscale and fine-quartz particles in rats: Toxicity is not dependent on particle size but on surface characteristics.** *Toxicological Sciences* 2007, 95:270-280.

101. Bermudez E, Mangum JB, Wong BA, Asgharian B, Hext PM, Warheit DB, Everitt JI: **Pulmonary responses of mice, rats, and hamsters to subchronic inhalation of ultrafine titanium dioxide particles.** *Toxicological Sciences* 2004, 77:347-357.

102. Veranth JM, Kaser EG, Veranth MM, Koch M, Yost GS: **Cytokine responses of human lung cells (BFAS-2B) treated with micron-sized and nanoparticles of metal oxides compared to soil dusts.** *Part Fibre Toxicol* 2007, **4.**

103. Ridker PM: **High-sensitivity C-reactive protein: Potential adjunct for global risk assessment in the primary prevention of cardiovascular disease.** *Circulation* 2001, **103**:1813-1818.

104. Toss H, Lindahl B, Siegbahn A, Wallentin L, Group ftFS: **Prognostic Influence of Increased Fibrinogen and C-Reactive Protein Levels in Unstable Coronary Artery Disease.** *Circulation* 1997, **96**:4204-4210.

105. Kofler S, Kickel T, Weis M: **Role of cytokines in cardiovascular diseases: a focus on endothelial responses to inflammation.** *Clinical Science* 2005, **108**:205-213.

106. HEI: **Understanding the Health Effects of Components of the Particulate Matter Mix: Progress and Next Steps.** Cambridge, MA: Health Effects Institute; 2002.

107. Slowing II, Vivero-Escoto JL, Wu C-W, Lin VSY: **Mesoporous silica nanoparticles as controlled release drug delivery and gene transfection carriers.** *Advanced Drug Delivery Reviews* 2008, 60:1278-1288.

108. Veranth J, Cutler NS, Kaser EG, Reilly CA, Yost GS: **Effects of cell type and culture media on interleukin-6 secretion in response to environmnetal particles.** *Toxicol In Vitro* 2008, **22**:498-509.

109. Peters K, Unger RE, Kirkpatrick CJ, Gatti AM, Monari E: **Effects of nano-scaled particles on endothelial cell function in vitro: studies on viability, proliferation and inflammation.** *J Mater Sci Mater Med* 2004, **15**:321-325.

110. Gojova A, Guo B, Kota R, Rutledge J, Kennedy I, Barakat A: **Induction of inflammation in vascular endothelial cells by metal oxide nanoparticles: effect of particle composition.** *Environ Health Perspect* 2007, **115**:403-409.

111. Chang JS, Chang KL, Hwang DF, Kong ZL: **In vitro cytotoxicity of silica nanoparticles at high concentrations strongly depends on the metabolic activity type of the cell line.** *Environ Sci Technol* 2007, **41**:2064-2068.

112. Steerenberg P, Zonnenberg J, Dormans J, Joon P, Wouters I, van Bree L, Scheepers P, Van Loveren H: **Diesel exhaust particles induced release of interleukin 6 and 8 by (primed) human bronchial epithelial cells (BEAS-2B) in vitro.** *Exp Lung Res* 1998, **24**:85-100.

113. Lin W, Huang Y-w, Zhou X-D, Ma Y: **In vitro toxicity of silica nanoparticles in human lung cancer cells.** *Toxicology and Applied Pharmacology* 2006, **217**:252-259.

114. Myllynen PK, Loughran MJ, Howard CV, Sormunen R, Walsh AA, Vahakangas KH: **Kinetics of gold nanoparticles in the human placenta.** *Reproductive Toxicology* 2008. **26**:130-137.

115. Chao SK, Hamilton RF, Pfau JC, Holian A: **Cell surface regulation of silica-Induced apoptosis by the SR-A scavenger receptor in a murine lung macrophage cell line (MH-S).** *Toxicology and Applied Pharmacology* 2001, **174**:10-16.

116. Iyer R, Holian A: **Involvement of the ICE family of proteases in silica-induced apoptosis in human alveolar macrophages.** *Am J Physiol Lung Cell Mol Physiol* 1997, 273:L760-767.

117. Lim Y, Kim **J,** Kim K, Chang **H,** Park Y, Ahn **B,** Phee Y: **Silica-induced apoptosis in vitro and in vivo.** *Toxicol Lett* 1999, **108**:335-339.

118. Thibodeau M, Giardina C, Hubbard AK: **Silica-induced Caspase activation in mouse alveolar macrophages is dependent upon mitochondrial integrity and aspartic proteolysis.** *Toxicol Sci* 2003, 76:91-101.

119. Santarelli L, Recchioni R, Moroni F, Marcheselli F, Governa M: **Crystalline silica induces apoptosis in human endothelial cells *in vitro.*** *Cell Biology and Toxicology* 2004. **20**:97-108.

120. Hu S, Zhao H, Yin XJ, Ma JKH: **Role of mitochondria in silica-induced apoptosis of alveolar macrophages: inhibition of apoptosis by rhodamine** 6g **and** *N*- **a c e t y l - L - c y s t e i n e.** *Journal of Toxicology and Environmental Health Part A* 2007, **70**:1403-1415.

121. Schubert D, Dargusch R, Raitano **J,** Chan S: **Cerium and yttrium oxide nanoparticles are neuroprotective.** *Biochem Biophys Res Commun* 2006, **342**:86-91.